Author's response

Dear Editor,

Thanks for your revision. We accepted the changes in the manuscript and we made also a better proofreading. We changed the Figure 3 adding the volcanological observations in order to easily understand the matches with the frequencies associated to periodicities.

On behalf of the authors
Sincerely,

Silvia Massaro

Cyclic activity of Fuego de Colima volcano (Mexico): insights from satellite thermal data and non-linear models

Silvia Massaro[1,2*], Antonio Costa[2], Roberto Sulpizio[1,3], Diego Coppola[4], Lucia Capra[5]

[1]Istituto per la Dinamica dei Processi Ambientali – Consiglio Nazionale delle Ricerche, Via R. Cozzi 53, 20125, Milan (Italy)
[2]Istituto Nazionale di Geofisica e Vulcanologia, Via D. Creti 12, 40128, Bologna (Italy)
[3]Dipartimento di Scienze della Terra e Geoambientali, Università di Bari, Via Orabona 4, 70125, Bari (Italy)
[4] Dipartimento di Scienze della Terra, Università di Torino, Via Valperga Caluso, 35, 10129, Turin (Italy)
[5]Centro de Geociencias UNAM, Campus Juriquilla, Queretaro (Mexico)

*Corresponding Author: Silvia Massaro (silvia-massaro@libero.it)

Abstract

The Fuego de Colima volcano (Mexico) shows a complex eruptive behaviour with periods of rapid and slow lava dome growth, punctuated by explosive activity. We reconstructed the weekly discharge rate average between 1998 and 2018 by means of satellite thermal data integrated with published discharge rate data. By using spectral and wavelet analysis, we found a multi-year long-, multi-month intermediate-, and multi-week short-term cyclic behaviour during the period of the investigated eruptive activity, as those of many others dome-forming volcanoes. We use numerical modelling in order to investigate the non-linear cyclic eruptive behaviour considering a magma feeding system composed of a dual or a single magma chamber connected to the surface through an elastic dyke developing into a cylinder conduit in the shallowest part. We investigated the cases in which the periodicity is controlled by i) the coupled deep-shallow magma reservoirs, ii) the single shallow chamber, and iii) the elastic shallow dyke when is fed by a fixed influx rate or a constant pressure. Due to the limitations of the current modelling approach, there is no single configuration that can reproduce all the periodicities on the three different time scales. The model outputs indicate that the observed multi-year periodicity (1.5-2.5 years) can be described by the fluctuations controlled by a shallow magma chamber with a volume of 20-50 km^3 coupled with a deep reservoir of ca. 500 km^3, connected through a deep elastic dyke. The multi-month periodicity (ca. 5 - 10 months) appears to be controlled by the shallow magma chamber for the same range of volumes. The short-term multi-week periodicity (ca. 2.5 - 5 weeks) can be reproduced considering a fixed influx rate or constant pressure at the base of the shallower dyke. This work provides new insights on the non-linear cyclic behaviour of Fuego de Colima, and a general framework for the comprehension of eruptive behaviour of andesitic volcanoes.

1. Introduction

Lava dome forming eruptions are relatively long-lived events, lasting from several months to several decades (e.g. Merapi, Indonesia, Siswowidjoyo et al., 1995; Kelut, Indonesia, De Bélizal et al., 2012; Fuego de Colima, Mexico, Lamb et al., 2014; Santiaguito, Guatemala, Harris et al., 2002), and usually punctuated by dome collapses and explosive (Vulcanian) episodes. Discharge rates can change widely over a range of time scales, reflecting the physical mechanisms involved in the transfer of magma to the Earth's surface (Melnik et al., 2008; Odbert and Wadge, 2009). Dome growth shows a periodic behaviour, which has been commonly observed at several volcanoes, including Santiaguito (Guatemala, Harris et al., 2003), Mt St Helens (USA, Swanson and Holcomb, 1990), and Soufrière Hills (Montserrat, Voight et al., 1998; Loughlin et al., 2010; Wadge et al., 2010; Nicholson et al., 2011). Periodic behaviours can be complex, showing systematic or non-systematic temporal changes as the eruption progresses (Denlinger and Hoblitt, 1999; Costa et al., 2007a; Melnik et al., 2008; Bernstein et al., 2013; Wolpert et al., 2016), and can be characterized by short-, intermediate- and long-term periodicities (Costa et al., 2007a; Melnik et al., 2008; Costa et al., 2012; 2013; Melnik and Costa, 2014). Short- and intermediate-term periodicities (hours or weeks) are generally explained by the upper conduit pressurization related to the non-linear ascent of magma flow (Denlinger and Hoblitt, 1999; Melnik and Sparks, 1999; Voight et al., 1999; Wylie et al., 1999; Ozerov et al., 2003; Lensky et al., 2004, Costa et al., 2007a,b; 2012; Kozono and Koyaguchi, 2009; 2012). This is because the lower part of the dyke-conduit can act as a capacitor that allows magma to be stored temporarily and released during the more intense phase of discharge (Costa et al., 2007a,b; Melnik et al., 2008; Costa et al. 2012; 2013). The long-term periodicity, with time scales from several months to decades (Voight et al., 2000; Belousov et al., 2002; Sparks and Young, 2002; Wadge et al., 2006), is usually controlled by pressure variations in magma reservoirs (Barmin et al., 2002; Costa et al., 2007b; Melnik et al., 2008; Melnik and Costa, 2014). Since historical times, the Fuego de Colima volcano (Mexico; Fig.1a) has been characterised by decade-lasting cycles of dome growth alternating with Vulcanian explosions, ended with sub-Plinian

eruptions (the last two occurred in 1818 and 1913; Luhr, 2002; Saucedo et al., 2005; Norini et al., 2010; Heap et al., 2014; Massaro et al., 2018a). The most recent cycle started after the 1913 eruption, and it is characterized by lava domes extruded with minor seismicity at high magma temperatures (960-1020°C; Savov et al., 2008). As for other dome eruptions (Sparks, 1997), dome growth at Fuego de Colima can be explained by complex non-linear pressure variations during magma ascent from magma reservoirs (e.g. Melnik and Costa, 2014), cooling, crystallization, degassing (e.g. Melnik and Sparks, 1999; Lensky et al., 2004; Nakanishi and Koyaguchi, 2008; Kozono and Koyaguchi, 2012) and upper conduit geometric configurations characterized by multiple pathways (e.g. Lavallée et al., 2012; Reubi et al., 2015).

Two magma chambers located at different depths characterize the feeding system of Fuego de Colima volcano (Fig. 1b), with roofs located at ca. 6 (shallow magma chamber) and ca. 15 km (deep magma chamber) of depth, as indicated by petrographic studies (Macìas et al., 2017) and geophysical data (Spica et al., 2017).

The purpose of this study is to investigate the existence of pattern of fluctuations in discharge rates during the 1998-2018 erupted activity at Fuego de Colima volcano. The available geological, geophysical, and petrological data for this recent activity provide a remarkable opportunity to improve the characterization and our understanding about the physical processes underlying cyclic extrusion of lava domes. In particular, we used thermal remote sensing data along with published effusion rates for reconstructing the oscillatory magma discharge rate behaviour of effusive activity at Colima.

The availability of satellite thermal images in the last decade has strengthened the use of thermal data for observing volcanic activity (e.g. Ramsey and Harris, 2012), especially in studying the relationships with lava discharge rates (Coppola et al., 2009; Harris et al., 2010; Garel et al., 2012). Coppola et al. (2013) propose that the radiant density of effusive/extrusive activity can be used to estimate lava discharge rates and erupted volumes by means of empirical relationship based on SiO_2 content of the erupted lava. Although it is still under debate, the so-called “thermal approach”

(Dragoni and Tallarico, 2009) offers a good way for monitoring volcanic activity, especially when direct observations are limited or absent. Here we focus our attention to the dynamics of fluctuations in magma discharge rate at different timescales at Fuego de Colima volcano during 1998-2018. By using time series analytical techniques (i.e. Fourier and wavelet analysis) we have identified three fundamental periodicities in subsets of the time series: i) long-term (ca. 1.5-2.5 years), ii) intermediate-term (ca. 5-10 months), iii) short-term (ca. 2.5-5 weeks), similar to those observed at many lava-dome eruptions (e.g. Costa et al., 2012; Melnik and Costa, 2014; Christopher et al., 2015). These periodicities were compared with numerical simulations provided by the model of Melnik and Sparks (2005) as generalized by Costa et al. (2007a) for accounting the presence of a shallow dyke, and Melnik and Costa (2014) for describing the control of a coupled dual chamber system. Numerical modelling of the different parts of the plumbing system can successfully reproduce the first-order cyclic behaviour of Fuego de Colima during the 1998-2018 erupted activity. Our results highlight that the dual magma chamber dynamics controls the long-term periodicity evident during 2002-2006 and 2013-2016, while the single magma chamber dynamics are more effective to explain the intermediate-term periodicity in the same periods. Finally, the shallow dyke dynamics regulate the multi-week cycles observed during 2002-2006 and 2011-2016.

The present work is divided in five main sections. The first describes the historical activity of the Fuego de Colima, with particular attention to the recent period, from 1998 to 2018. The second section describes the methods applied to the dataset composed of the satellite thermal data integrated with published data. The third section is dedicated to the input and target data used for numerical simulations. The fourth section presents the results obtained by the spectral and wavelet analyses. This latter allows us to establish significance levels for the wavelet power spectrum. The periodicities observed in this spectrum were compared to the results obtained by numerical simulations. The last fifth section contains a discussion on the eruptive behaviour occurred at Fuego de Colima during 1998-2018, providing new insights from the observed data and non-linear models.

2. The historical activity of Fuego de Colima volcano

Since historical times Fuego de Colima represents the most active volcano in Mexico, posing a serious threat to all surrounding populations (Cortés et al., 2005; Gavilanes-Ruiz et al., 2009; Bonasia et al., 2011; Roverato et al., 2011). The earliest accounts of the volcano activity can be found in Historia Antigua de Mexico (Clavijero, 1780), where the destructive effects of its explosive activity are carefully described (Bretón-Gonzales et al., 2002). The historical activity of Fuego de Colima was described and interpreted by several authors (Luhr and Carmichael, 1980; Medina-Martínez, 1983; De la Cruz-Reyna, 1993; Bretón-Gonzales et al., 2002; Luhr, 2002). The Fuego de Colima has shown a transitional eruptive behaviour spanning from effusive to explosive activity, dominated by dome growth and Vulcanian eruptions. Occasionally sub-Plinian events occurred (1576, 1606, 1690, 1818 and 1913), indicating a recurrence time of approximately 100 years (De la Cruz-Reyna, 1993; Luhr, 2002; Saucedo et al., 2005; Gavilanes-Ruiz et al., 2009; Massaro et al. 2018a). The sub-Plinian event occurred in 1913 (Saucedo et al., 2010) is the largest historical eruption and it has been used as benchmark for volcanic hazard studies (Martin Del Pozzo et al., 1995; Saucedo et al., 2005; Bonasia et al., 2011).

2.1. The 1998-2018 eruptive activity

The 1998-2018 is the only period of post 1913 activity for which there is sufficiently available information to explore the cyclic activity of Fuego de Colima. Different periods of effusion (domes and lava flows) punctuated by Vulcanian eruptions and dome collapses characterised the volcano activity between 1998 and 2018 (Savov et al., 2008; Varley et al., 2010a; Hutchinson et al., 2013; Mueller et al., 2013; Zobin et al., 2015; GVP, 2017). The duration of extrusive activity and magma discharge rate varied through time, that was generally divided into five eruptive phases up to 2015; I) 1998-1999; II) 2001-2003; III) 2004-2005; IV) 2007-2011; V) 2013-2015 (Zobin et al., 2015; Aràmbula-Mendoza et al., 2018).

The first dome extrusion of the 1998-1999 phase started in November 1998, and quickly filled the 1994 explosion crater, forming lava flows that descended the southern flanks of the Fuego de Colima cone during most of 1999 (> 5 m^3 s^{-1} in average for Mueller et al., 2013; 4.11 m^3 s^{-1} in average for Reubi et al., 2013).

At the beginning, this dome grew rapidly (ca. 4.4 m^3 s^{-1}) reaching a volume of ca. 3.8 × 10^5 m^3 in 24 hours. During this period the effusion rate reached a peak value around 30 m^3 s^{-1} (Navarro-Ochoa et al., 2002; Zobin et al., 2005; Reubi et al., 2015) and showed a cyclic damped behaviour soon after. During 1999-2001 a series of explosions destroyed the dome and excavated a large apical crater (Bretòn-Gonzales et al., 2002).

A slow outpouring of lava (< 1 m^3 s^{-1} for Mueller et al., 2013; 0.17 m^3 s^{-1} for Reubi et al., 2013; 2015) resumed in May 2001 and continued for 22 months. In February 2002, the lava dome overflowed the crater rims producing lava flows. During this eruptive phase, the magma extruded from three separate vents with only minor explosive activity, at a rate of ca. 0.9 m^3 s^{-1} (GVP, 2002). Vulcanian explosions dismantled the dome during July and August 2003 (GVP, 2003).

In September 2004, low-frequency seismic swarms heralded the onset of the new effusive phase (Varley et al., 2010a; Arámbula-Mendoza et al., 2011; Lavallée et al., 2012) with a small increase in average discharge rate of 0.6 m^3 s^{-1} (Reubi et al., 2013; 2015). The lava dome building occurred from the end of September until the beginning of November, with a magma effusion rate up to 7.5 m^3 s^{-1} in October (Zobin et al., 2008; 2015). The effusive activity was accompanied and followed by intermittent Vulcanian explosions. The explosive activity diminished in intensity during December 2004-January 2005. From February to September 2005, effusion and large explosions occurred.

In the following months, small, short-lived domes were observed, with an estimated effusion rate between 1.2 – 4.6 m^3 s^{-1} (Varley et al., 2010b; Reubi et al., 2015). In May and June, the explosive activity produced pyroclastic density currents reaching distances up to 5.4 km from the volcano summit (Varley et al., 2010a). In February 2007, a new lava dome began to grow and explosions

were reported in the period between January 2009 and March 2011. The 2007-2011 period of dome extrusion represents the slowest growth rate in the recent history of Fuego de Colima. Hutchinson et al. (2013) calculated a mean effusion rate of ca. 0.02 m^3 s^{-1} from 2007 to 2010 using digital photographic data, in good accordance with Zobin et al. (2015) that reported extrusion rates of 0.03 m^3 s^{-1} during 2007. Mueller et al. (2013) estimated the magma extrusion rate between 0.008 ± 0.003 m^3 s^{-1} to 0.02 ± 0.007 m^3 s^{-1} during 2010, which dropped down to 0.008 ± 0.003 m^3 s^{-1} again in March 2011. On 21 June 2011 an explosion heralded the cessation of dome growth and marked the end of the effusive period.

After 1.5 years of rest, in January 2013 a sequence of explosions cored out the 2011 dome and generated pyroclastic density currents that reached distances of up to 2.8 km from the summit (GVP, 2013). From March to October, the calculated discharge rate was in the range of 0.1 – 0.2 m^3 s^{-1} (Reyes-Dàvila et al., 2016). Successively, the mid-low explosive activity took place up to February-March 2014, until a new pulse of magma observed in July, with an approximate rate of 1-2 m^3 s^{-1} (Aràmbula-Mendoza et al., 2018). On 11 January 2015, a new lava dome was observed inside the crater (Thiele et al., 2013) and its growth continued until July, with effusion rate of ca. 0.27 m^3 s^{-1} (Zobin et al., 2015). Between 10-11 July 2015 the recent dome was destroyed by the most intense activity since the 1913 eruption (Capra et al., 2016; Reyes-Dávila et al., 2016). In the 2013-2015 period, the average extrusion rate was of ca. 0.2 m^3 s^{-1} (Thiele et al., 2017), with peak values > 10 m^3 s^{-1} (Varley, 2015). After that, the eruptive activity ceased until January 2016 when daily ash plumes started to occur along with active lava flows and explosions. In early July a new dome began to grow, overtopping the crater rim. A large explosion was recorded on 10 July 2016, followed by daily and multiple-daily ash plumes up to the end of year. Multiple flows descended from lava dome during September-December. In 2017 frequent strong explosions and ash emissions were recorded until March. Through June decreasing seismicity and minor landslides were reported with no evidence of effusive activity or new dome growth (GVP, 2017). Here we provide a more systematic overview of the 1998-2018 erupted activity, obtained by satellite thermal data along with

some published data, explained in the following section.

3. Methods

We analysed the thermal energy spectrum of Fuego de Colima volcano available from March 2000 to October 2018, detected Middle Infrared Observation of Volcanic activity (MIROVA) hot-spot detection system (Coppola et al., 2016). The period 1998-1999 was integrated using published discharge rates (Navarro-Ochoa et al., 2002; Zobin et al., 2005). The MIROVA NRT system is based on the near real time (NRT) analysis of the MODerate resolution Imaging Spectroradiometer (MODIS) data, distributed by the LANCE-MODIS data system (http://modis.gsfc.nasa.gov/).

The thermal emission from an object is attenuated by the atmosphere resulting from absorption by gases and scattering by particles. MIROVA system focuses on the Middle InfraRed region (MIR), which shows the lowest attenuation levels, to better detect and analyse thermal radiation emitted from volcanic sources. While the standard MODIS forward processing delivers Aqua and Terra images within 7-8 hours of real time, LANCE-MODIS allows for the creation of MIROVA radiant flux time series within 1-4 hours from the satellite overpass (www.mirovaweb.it). This thermal data collection was converted into lava discharge rate estimates and integrated with some published data in order to reconstruct the weekly mean discharge rate spectrum from 1998 to 2018 (Fig. 2a).

In this work, we refer to Coppola et al. (2013), who describes the relationship between the heat lost by lava thermal radiance variations and discharge rates, by means of a unique, empirical parameter. They compared the energy radiated during several distinct eruptions to the erupted lava volumes (m^3). The relationship between the Volcanic Radiated Energy (*VRE*) and the erupted volume was defined by introducing the concept of radiant density (c_{rad}, in J m^{-3}). This parameter is analysed as a function of the SiO_2 content and the bulk rheological properties of the related lava bodies. It is strongly controlled by the characteristic thickness of the active lavas at the time of a satellite overpass, whereas the effects of variable degree of insulation, morphology and topographic

conditions produce only a limited range of variability (± 50%) (Coppola et al., 2013). For the Fuego de Colima we used a value of c_{rad} = 3.90 × 10^7 (J m^{-3}) for a SiO_2 content of 59.6% (Savov et al., 2008; Coppola et al., 2013). We obtained the cumulative volumes of effusion per year (from 2000 to 2018) considering the ratio between the average *VRE* estimations and c_{rad}. It is important to stress that the instrumental limit of the MIROVA system is not able to detect thermal anomalies below 0.5–1 MW. Since we used a radiant density (c_{rad}) of 3.90 × 10^7 J m^{-3}, the minimum reliable value of discharge rate is 0.01 m^3 s^{-1} (Coppola et al., 2013). As reported by Coppola et al. (2016), the thermal data obtained from MIROVA are not corrected due to the presence/attenuation of clouds. For this reason, the estimates of effusion rates and volumes are to be considered as minimum estimates.

Because the 2002-2006 and 2013-2016 intervals are the most active in the analysed period, we firstly applied the Fourier analysis to the monthly average of discharge rates (Fig. 2b) of these time intervals, in order to explore the modal spectrum of the signal. Although Fourier analysis is well suited to the quantification of constant periodic components in a time series, it cannot recognise signals with time-variant frequency content. Whereas a Fourier Transform analysis may determine all the spectral components embedded in a signal, it does not provide any information about timing of occurrence. To overcome this problem, several solutions have been developed in the past decades that are able to represent a signal in the time and frequency domain at the same time.

The aim of these approaches is to expand a signal into different waveforms with local time–frequency properties well adapted to the signal structure (Cazellas et al., 2008). In order to get information on the amplitude of the periodic signals within the Fuego de Colima (MIROVA) time series, we performed a wavelet analysis by decomposing the weekly time series (Fig. 2a) into time/frequency space (Fig. 3).

Wavelet analysis is a powerful tool largely used in many scientific fields (i.e., ecology, biology, climatology, geophysics) and engineering. It is especially relevant to the analysis of non-stationary

systems (i.e., systems with short-lived transient components, Cazellas et al., 2008). In particular, the wavelet analysis is well suited for investigations of the temporal evolution of aperiodic and transient signals (Lau and Weng, 1995; Mallat, 1998).

For this study, practical details in applying wavelet analysis were taken from Torrence and Compo (1998) and Odbert and Wadge (2009). It is worth noting that wavelet analysis considers a wave that decays over a finite time and whose integral over infinite time is zero. Many forms of wavelet (called "wavelet functions" $\psi(\eta)$, or "mother functions", which depend on a non-dimensional time parameter "η") have been designed for analytical use (Farge, 1992; Weng and Lau, 1994; Daubechies, 1994), each with its own characteristics that make it suitable for certain applications. The choice of the wavelet can influence the time and scale resolution of the signal decomposition. Wavelet analysis is popular in geosciences (Trauth, 2006) as it does not require any a priori understanding of the system generating the time series.

Our time series (weakly average discharge rates acquired mainly by the MIROVA system; Fig. 2a), called (x_n), has equal time spacing (δt = 7 days) and number of points n = 0…N-1. Using the approximately ortohogonal Morlet function as wavelet function $\psi(\eta)$ (it must have zero mean and be localized in both time and frequency space; Farge, 1992), we here define the wavelet transform $W_n(s)$ as the convolution of x_n with a scale (s) and translated version of $\psi_0(\eta)$ (mother function). In formula:

$$W_n(s) = \sum_{n'=0}^{N-1} xn' \psi * \left[\frac{(n' - n)\delta t}{s}\right] \quad (1)$$

where the (*) indicates the complex conjugate. The scale s should be equal to approximately $2\delta t$, according to the Nyquist theorem. Therefore, the smallest wavelet we could possibly resolve is $2\delta t$, thus we choose s_0 = 14 days. Generally, $\psi(\eta)$ is a complex function, therefore the wavelet transform is also complex. It is possible to reconstruct the "local" wavelet power spectrum as the absolute-

value squared of the wavelet coefficients, $|Wn(s)|^2$. The way to compute the wavelet transform for a time series is to find the Fourier transform of both the wavelet function (Morlet in our case) and the time series. Following Torrence and Compo (1998), we made the normalization by dividing by the square-root of the total wavelet variance (σ^2).

Usually, a periodic component in a time series may be identified in a power spectrum if it has distinctly greater power than a mean background level (that would correspond to a Gaussian background noise) (Odbert and Wadge, 2009). However, the spectra generated from many geophysical systems indicate that the noise in time series data tends not to have a Gaussian distribution (Vila et al., 2006) but it can be better described by coloured noise, specifically red noise (Fougere, 1985). For this reason, we use a simple model for red noise given by the unvariate lag-1 autoregressive or Markov process (Torrence and Compo, 1998) in order to determine the significance levels for our wavelet spectrum. These background spectra are used to establish a null hypothesis for the significance of a peak in the wavelet power spectrum. The null hypothesis is defined for the wavelet power spectrum considering that the time series has a mean power spectrum: if a peak in the wavelet power spectrum is significantly above this background spectrum, then it can be assumed to be a true feature with a certain percentage of confidence. For definitions, "significant at the 5% level" is equivalent to "the 95% confidence level" (Torrence and Compo, 1998). The confidence interval is defined as the probability that the true wavelet power at a certain time and scale lies within a certain interval about the estimated wavelet power (Torrence and Compo, 1998). Because we deal with finite-length time series, errors occur at the beginning and end of the wavelet power spectrum. A solution is to pad the end of the time series with zeroes to bring the total length N up to the next-higher power of two, thus limiting the edge effects. However, padding with zeroes introduces discontinuities at the endpoints and, especially towards larger scales, decreasing the amplitude near the edges as more zeroes enter the analysis (Torrence and Compo, 1998). The cone of influence (COI) is the region of the wavelet spectrum beyond which

edge effects become important. The criterion for applying wavelet analysis is very similar to those employed with classic spectral methods. In other words, the wavelet transform can be regarded as a generalization of the Fourier transform, and by analogy with spectral approaches, we compute the local wavelet power spectrum as described above. Successively, this can be compared with the "global" wavelet power spectrum which is defined as the averaged variance contained in all wavelet coefficients of the same frequency (Torrence and Compo, 1998; Cazellas et al., 2008).

Numerical simulations have been carried out using the magma flow model of Melnik and Costa (2014), who generalized the model proposed by Melnik and Sparks (2005) and Costa et al. (2007a) for a magma chamber connected to a dyke that develops into a cylindrical conduit near surface. In particular, the model of Melnik and Costa (2014) accounts for the possibility of a dual magma chamber system. The model accounts for rheological changes due to volatile loss and temperature driven crystallization. These processes are both effective during dome extrusion eruptions because of the typical low magma ascent velocities (from millimetres to few centimetres per second), which can result in magma transit times from days to weeks. These ascent times are often comparable with those of crystal nucleation and growth (Melnik and Sparks, 1999; 2005; Costa et al., 2007c).

4. Input and target data for numerical simulations

4.1 Geometrical configurations of the magma plumbing system

Within the physical framework used in the Melnik and Costa (2014), the model (Fig. 1b) consists of two elastic magma chambers located at different depths, with chamber pressures P_{chs} and P_{chd} able to drive the magma ascent in elliptical cross-section volcanic conduit (approximating a dyke). Near surface the conduit develops into a cylinder at depth L_T (named "transition level").

Numerical simulations were carried out considering the shallower magma chamber (single magma chamber configuration) or the double magma chamber. The single magma chamber model

316 considers a conduit feeding system composed of a shallow dyke (d_s) that connects the magma
317 chamber to a shallower cylinder, in agreement with geological and geophysical evidence from
318 different volcanoes (Melnik and Sparks, 2005; Costa et al., 2007a; Melnik et al., 2008; Melnik and
319 Costa, 2014). The double magma chamber model includes the addition of a deep reservoir
320 connected to the shallow chamber through a deep elastic dyke (d_d) (Fig. 1b).
321 In order to reproduce the observed fluctuations in discharge rates recorded in some periods of the
322 1998-2018 erupted activity, we considered a discharge rate regime where the period of pulsations is
323 controlled by the elasticity of the shallow dyke, and a discharge rate regime where the periodicity is
324 controlled by the volume of the single or dual magma chamber(s) (Barmin et al., 2002; Melnik and
325 Sparks, 2005; Costa et al., 2007a; Melnik and Costa, 2014).
326 In Appendices A1 and A2 we reported some test simulations in order to show the control of the
327 most sensitive parameters (i.e. water content in magma, dyke dimensions, volume of magma
328 chamber, magma influx rate into the magma chamber) affecting the model outputs in case of the
329 single magma chamber model. The volumes of the magma chamber (V_{ch}) range from 20 to 50 km^3
330 and the width of the feeder dyke $2a$ varies from 200 to 400 m (Massaro et al., 2018a).
331 In Appendix A3 is shown the sensitivity test aimed to explore a broad range of chamber volumes
332 and aspect ratios in the case of double magma chamber configuration. The deep chamber has its top
333 at 15 km of depth, it is pressurised and fed from below by a constant influx $Q_{in,d}$. The volumes of
334 shallow magma chamber (V_{chs}) range from 30 to 50 km^3, and the volumes of the deep magma
335 chamber (V_{chd}) from 550 to 750 km^3, according to geophysical data (Cabrera-Espindola, 2010;
336 Spica et al., 2017). The aspect ratios for shallow and deep magma chambers (AR_s - AR_d) varied
337 from 1 to 2. For each run included in the sections 1-3 of A4, we used a fixed influx $Q_{in,d}$ =2.3 m^3 s^{-1},
338 and variable widths of the deeper dyke ($2a_{0d}$) from 200 to 3000 m (representative from weak to
339 strong coupling of the magma chambers; Melnik and Costa, 2014). The lower dyke thickness $2b_{0d}$ is
340 not an input data of the model as it changes as function of local pressure conditions, therefore it
341 does not appear in the diagrams. In Section 4 of A3 we show two sets of runs having $Q_{in,d}$ equal to

1 and 3 $m^3 s^{-1}$ respectively, and the following fixed parameters: AR_s and AR_d = 1, V_{chd} = 650 km^3, V_{chs} = 40 km^3.

4.2 Petrological data

Erupted products at Fuego de Colima are chemically intermediate and primarily andesitic lavas with ca. 61 wt.% SiO_2, (Lavallè et al., 2012). The observed dome growth phases are usually fed by prolonged magma ascent times, which allow efficient degassing and crystallization. This is in agreement with the low mean porosity (14-16% e.g Lavallè et al., 2012; Farquharson et al., 2015) and low water contents of the products of the recent activity (2 wt. % for 1998-1999, Mora et al., 2002; 0.1-2.5 wt. % for 1998-2005 products, Reubi and Blundy, 2008). Dome lava currently erupted exhibits a range of crystallinities (phenocrysts, 20–30 vol.%; microlites, 25–50 vol.%), and the groundmass constitutes as much as 68 vol.% (Luhr, 2002). The andesites show a porphyritic texture with plagioclase (13–25 vol.%), orthopyroxene (2– 4 vol.%), clinopyroxene (3–4 vol.%) and minor hornblende (<0.5%) and Fe–Ti oxides (ca. 2 vol.%). Olivine occurs rarely as xenocrysts (Lavallè et al., 2012).

As reported in Melnik and Costa (2014), the magma viscosity μ is calculated according to Costa et al. (2007a) considering the melt viscosity, μ_m, times a correction for the effects of crystallinity, θ, and for the bubbles, η. In formula:

$$\mu = \mu_m(c, T)\, \theta(\beta)\, \eta(\alpha, Ca) \quad (2)$$

which depends on the melt viscosity μ_m (that is function of the water content c and temperature T), on the crystal content β, on bubble fraction α and on bubble capillarity number Ca. The rheological model is described in detail in Costa et al. (2007a). Table 1 summarises the value ranges used for the input parameters of the model.

5. Results

In Figure 2 we showed the averages of discharge rates at Fuego de Colima volcano from November 1999 to October 2018. Here we define as "high" discharge rates values > 0.1 $m^3 s^{-1}$ (highlighted as dark blue areas). All values below 0.1 $m^3 s^{-1}$ are considered "low" discharge rates (light blue areas). Volcanological observations are reported at the top and the bottom of the diagram. It is worth noting that the "high" and "low" explosive activity correspond to the high and low discharge rate, respectively. In addition, we distinguished between lava flows and lava domes accordingly to the dominant emplacement style typical of each eruption, and between "low" (i.e. ash plumes, gas emissions) and "high" (i.e. strong explosions, Vulcanian eruptions) magnitude explosive activity.

The weekly average of discharge rates represents the complete dataset used in this study, and is reported in Figure 2a. These data have been calculated by using the MIROVA data (black dots) for the 2000-2018 period, and complemented with published data (blue crosses) for the 1998-1999 period (Navarro-Ochoa et al., 2002; Zobin et al., 2005). Even if the data detection of satellite thermal energy represents a continuous spectrum of information, it is worth noting that it suffers of some limitations connected to cloud covering, magma composition, rheology, and emplacement of the investigated lava body due to topographic conditions (Harris and Rowland, 2009; Harris et al., 2010; Coppola et al., 2013). Figure 2b shows the monthly discharge rate spectrum from 1998 to 2018 using the MIROVA dataset (black dots), integrated with available published data (blue crosses) (Navarro-Ochoa et al., 2002; Zobin et al., 2005; Capra et al., 2010; Varley et al., 2010a; Sulpizio et al., 2010; James and Varley, 2012; Hutchinson et al., 2013; Reubi et al., 2013; Varley, 2015; Reyes-Dávila et al., 2016; Thiele et al., 2017; GVP, 2000; 2017). Figure 2c summarizes the yearly average of discharge rates from MIROVA dataset, highlighting the good agreement with the available average estimation of yearly discharge rates from literature (Mueller et al., 2013; Reyes-Dàvila et al., 2016; Aràmbula et al., 2018; GVP, 1998-2017).

5.1 Fourier analysis

We applied Fourier analysis to the 1998-2018 dataset (Fig. 2a). In particular, we chose two time windows: i) 2002-2006 period which showed two periodic components, T_0 = 24.70 and T_1 = 6.17 corresponding to ca. 24 and ca. 6 months, respectively (Appendix A4 Fig. a), and ii) 2013-2016 period that provided similar results: T_0 = 24. 94 and T_1 = 6.23 corresponding to ca. 25 and ca. 6 months, respectively (Appendix A4, Fig. b).

5.2 Morlet wavelet analysis

The whole analysed dataset is composed of 825 data points, representing the time evolution of the oscillating components of the 1998-2018 eruptive activity (Fig. 2a). Figure 3a shows the normalised local wavelet power spectrum of the signal. The colours scale for power values vary from light orange (low values) to dark red (high values). The thick black contours represent the 95% confidence level. The blue line indicates the cone of influence (COI) that delimits the region not influenced by edge effects. From this analysis, it is easy to observe three main periodicities during 2002-2006 and 2013-2016 periods: i) long-term periodicity of ca. 1.5–2.5 years; ii) intermediate-term periodicity of ca. 5-10 months; and, iii) short-term periodicity of ca. 2.5-5 weeks. The volcanological observations (about “high” and “low” discharge rates) are also reported in order to provide a closer link between the observational datasets and the identification of frequency change in the extrusion rate time series. The short-term periodicity is also present in 2011 (Fig. 3a). Figure 3b shows the global wavelet spectrum corresponding to the local wavelet power spectrum plotted in Fig. 3a. The green dashed line shows the position of the best-fitting red noise model at the 95% confidence level.

5.3 Numerical simulations

Appendices A1-A3 provide some sensitivity tests in order to explore the effects of different parameters on discharge rate fluctuations for the single (A1-A2) and dual magma chamber models (A3). In particular, in Appendix A1 is reported the general steady-state solution of the numerical model, with both stable and unstable branches (e.g. Melnik et al., 2008; Nakanishi and Koyaguchi, 2008), showing that the cyclic behaviour can occur only between 2 and 4 m^3 s^{-1}, for the fixed input data (panel (a)). Varying the width of the shallow dyke *2a* (from 200 to 400 m) and water content in the melt phase, we observed how the unstable branch changes its shape. This implies different periods of possible oscillations in discharge rate (panels (b)-(c)).

Appendix A2 provides a set of simulations carried out varying the width of the shallow dyke *2a* (panel (a)). The resulting periodicities vary from ca. 1000 days (*2a* = 200 m) ca. 500 days (*2a* = 300 m) to ca. 250 days (*2a* = 400 m). These results highlight negative correlation between dyke widths and periods of oscillation (Costa et al., 2007a). In this case, the variable widths influence the intensity and periodicity of discharge rates: the wider the dyke, the lower the intensity and periodicity of discharge rates. Differences in the amplitude of oscillations are observed in panel (b), highlighting a positive correlation between the volume of the magma chamber V_{ch} and periodicities. Periodicities of ca. 500 days correspond to 20 - 30 km^3, while larger values of ca. 970 and ca. 1176 days are provided for 40 and 50 km^3, respectively. In panel (c), we reported also a set of simulations considering the modelled discharge rate controlled by the elasticity of the shallower dyke with fixed influx rates Q_{in} (in the range of 0.01 - 0.1 m^3 s^{-1}).

Appendix A3 contains four sections dedicated to the sensitivity tests for the dual magma chamber model. As reported in Melnik and Costa (2014), the dual chamber model shows cyclic behaviour with a period that depends on the intensity of the influx rate and the chamber connectivity (described as the horizontal extent of the dyke connecting the two chambers). For a weak connectivity, the overpressure in the deeper chamber remains nearly constant during the cycle and

the influx of fresh magma into the shallow chamber is also nearly constant. For a strong connectivity between the two chambers, their overpressures increase or decrease during the cycle in a synchronous way. Influx into the shallow chamber stays close to the extrusion rate at the surface (Melnik and Costa, 2014). We explored different cases considering various fixed parameters as follow: *i*) volumes of the shallow and deep magma chambers (V_{chs} = 40 km^3, V_{chd} = 650 km^3); *ii*) aspect ratios (AR_s = 1, AR_d = 1) and the deep magma chamber volume (V_{chd} = 650 km^3); *iii*) aspect ratios (ARs = 1, ARd = 1) and the shallow magma chamber volume (V_{chs} = 40 km^3). For *i*), *ii*) and *iii*) cases, the deep influx rate $Q_{in,d}$ has fixed values from 3 to 1 m^3/s. In conclusion, these sensitivity tests showed the passage from weakly connected magma chambers (lack of simultaneous oscillation of $Q_{in,s}$ and Q_{out}) when $2a_{0d}$ = 200 m to strongly connected magma chambers (synchronous oscillations of $Q_{in,s}$ and Q_{out}) when $2a_{0d}$ = 3000 m.

Figure 4 reported the results of numerical simulations aimed to reproduce the Fuego de Colima fluctuations during 1998-2018. Figure 4a shows a representative example of time-dependent solution for a discharge rate controlled by the elasticity of the shallower dyke. Simulations were carried out using fixed values of pressure (blue line) and influx rate (green line) at the source region of the shallower dyke, which is ca. 6000 m long. The dyke has width $2a$ = 400 m and thickness $2b$ = 2 m and a dyke-cylinder transition *TL* at 1300 m of depth. The magma chamber volume is fixed to 30 km^3. Solutions present periodicities from 16 to 40 days in agreement with the weekly periodicities of ca. 38-18 days (ca. 2.5-5 weeks) derived from the wavelet analysis (Fig. 3a).

Figure 4b describes a representative example of the single magma chamber model simulations. We set the magma feeding system composed of a dyke long 6500 m, having a width $2a$ = 600 m, thickness $2b$ = 4 m, and a dyke-cylinder transition *TL* fixed at 1000 m of depth. The chamber has a volume fixed to 30 km^3 and receives a constant $Q_{in,s}$ = 2.3 (m^3 s^{-1}). The transient solution is accounted for the discharge rate controlled by the magma chamber volume, showing an intermediate-term periodicity of ca. 220 days, in agreement with the intermediate-term periodicity of ca. 146-292 days (ca. 5-10 months) obtained from the wavelet analysis (Fig. 3a).

Figure 4c reports a representative example of the solution obtained with the dual magma chamber model in order to assess the effect of the deep chamber on the discharge rate. We fixed the volumes of deep and shallow magma chamber at 40 and 650 km^3, respectively. The shallow dyke is 6500 m long with a width $2a$ = 260 m and thickness $2b$ = 4 m. The deep dyke has a width $2a_{0d}$ = 500 m and a deep influx rate $Q_{in,d}$ = 2.3 (m^3 s^{-1}). A cyclic behaviour of ca. 825 days is observed, reaching a peak discharge rate of ca. 6 (m^3 s^{-1}). This result is in agreement with the long-term periodicity of ca. 547-913 days (ca. 1.5 - 2.5 years) derived from the wavelet analysis (Fig. 3a).

Considering uncertainties in both modelling results and parameters and the fact that the thickness and width of the dykes are function of the local overpressure, results are quite consistent, although with a single model configuration the current approach cannot reproduce at the same time the periodicity observed at different time scales.

6. Discussions

In recent years, many studies have focused on magma flow dynamics in volcanic conduits during lava dome building eruptions (Melnik and Sparks, 1999; Wylie et al., 1999; Barmin et al., 2002; Melnik and Sparks, 2002; 2005; Costa et al., 2007a,b; Nakanishi and Koyaguchi, 2008; Kozono and Koyaguchi, 2012), highlighting periodic variations in discharge rate due to the transition from low regime (allowing efficient crystals growth leading to an increase in magma viscosity) to high regime (with negligible crystallization). This difference in discharge rates can be of orders of magnitude, with strongly non-linear responses to the variation of governing parameters from the volcanic system. This behaviour allows periodic oscillations of the discharge rate (Nakada et al., 1999; Watts et al., 2002), as observed in different dome extrusion eruptions (e.g. Mt St. Helens, Santiaguito, Soufrière Hills; Melnik et al., 2008). Although each volcano usually shows its complex pattern of discharge fluctuations, the cause can be explained as the superimposition of long,

492 intermediate, and short-term effects of the coupled magma chamber(s) and conduit dynamics. The
493 long-term oscillations in discharge rate are function of magma chamber size, magma
494 compressibility, amount and frequency of magma recharge and withdrawal (Barmin et al., 2002;
495 Costa et al., 2007b; Melnik et al., 2008; Costa et al., 2013). The short-term and intermediate
496 oscillation dynamics can also superimpose to the main long-term periodicity, through small changes
497 in magma temperature, water content, and kinetic of crystallization during magma transit in the
498 conduit (e.g., Melnik et al., 2008). The aforementioned eruptive behaviour characterized also the
499 Fuego de Colima activity in the 1998-2018 period, as demonstrated by the wavelet analysis of
500 satellite thermal data. It is important to stress that the oscillating behaviour is not regular, having a
501 period, between 2007 and 2012, that does not show any significant periodicity (Fig. 3a), possibly
502 indicating a damped oscillation (Appendix A2). During this period the volcano enter in an almost
503 quiescent status with very low discharge rates. This period of low discharge rates is punctuated by
504 low explosive activity, triggered by dome collapse or pressurization of the upper conduit.
505 It is well known for Fuego de Colima that Vulcanian explosions can evacuate significant portions of
506 the upper conduit and destroy the lava dome. The influence of these processes on the periodicity of
507 at least short-term periodic regimes could be significant. However, it is expected that such
508 processes should affect mainly sub-daily periodicities, as explained by Costa et al. (2012) who
509 analysed the periodicity variations due to the collapse of 200 m high plug at Montserrat. These
510 changes should also have significant effects on the multi-week periodicity analysed here. Certainly,
511 it is not excluded that an exceptional large evacuation of the upper conduit would be able to
512 influence longer periodicities as those investigated here, causing a transition to a more explosive
513 eruptive style (i.e. Plinian) (Massaro et al., 2018a).
514 In order to investigate the relationship between the periodic components observed in wavelet
515 analysis and the dynamics of the Fuego de Colima feeding system, we run simulations using the
516 numerical model Melnik and Costa (2014) (Fig. 4). The model can reproduce the results of the
517 wavelet analysis in terms of observed periodicities, allows us to relate short-, intermediate- and

518 long-term oscillations in discharge rates to the dynamics of upper conduit, shallow magma
519 chamber, and coupled shallow and deep magma chambers, respectively. This implies that the
520 pressurization of the deep magma chamber has cascade effects on the whole feeding system of the
521 Fuego the Colima, similarly to what observed in other recent lava dome eruptions (i.e. Montserrat;
522 (Melnik and Costa, 2014). It is of particular interest that the best output with the dual magma
523 chamber model indicates that chambers do not oscillate simultaneously ("decoupled oscillation";
524 Fig. 4c). Although the presented data provide, for the first time, a framework able to describe the
525 periodic behaviour of effusive activity at Fuego de Colima volcano, both numerical model and
526 wavelet analysis suffer of some limitations that need to be taken into account in interpreting the
527 results:

528 *i)* the available data of discharge rates and dome volumes collected for the 1998-2018
529 period do not have the same quality. For this reason, this lead us to extract only averages of
530 discharge rate for the entire period, with biasing effects to lower amplitudes;

531 *ii)* a common weakness of the spectral and wavelet analysis techniques is their inability to
532 distinguish the source of any given periodic component (i.e. whether it is a signal from a
533 volcanic process, an external process or if it is noise in the dataset). Elucidating the exact
534 mechanism requires competing robust models and multiple independent field observations
535 (Odbert and Wadge, 2009);

536 *iii)* assumptions behind the numerical model imply several limitations, such as those due to
537 the constant value of the dyke width and simplified Newtonian rheology. The first
538 assumption greatly oversimplifies the physics. In the case of large overpressures, stress at
539 the dyke tips will exceed the fracture toughness of the rocks and the dyke will expand
540 horizontally (Massaro et al., 2018b), reaching some equilibrium configuration. When the
541 deep chamber deflates, overpressure in the deeper dyke will decrease and, as flow rate
542 decreases, magma at the dyke tips can solidify, leading to a decrease in $2a_{0d}$ (Kavanagh and
543 Sparks, 2011; Melnik and Costa, 2014). Thermal exchange with wall rock can also affect

the nonlinear dynamics of the system (Costa and Macedonio, 2002; Melnik et al., 2008). In addition, a more realistic estimate of the magma viscosity during lava dome eruptions should account for the coupling with energy loss, viscous dissipation, and stick–slip effects (e.g. Costa and Macedonio, 2005; Costa et al. 2007c; 2013).

Although this study revealed that different periodic signals are controlled by different mechanisms occurring in the plumbing system, the current model approach is not able describe the three periodicities (long-, intermediate- and short-term) using a unique model configuration. Nevertheless, we hope this work will motivate further numerical modelling approaches in order to develop more sophisticated models able to describe the three time scales together, by incorporating further physical aspects (e.g. full thermal effects) and considering fully 3D geometries.

7. Conclusions

The coupling of wavelet analysis and numerical modelling allowed to decipher the eruptive behaviour of Fuego de Colima in the period 1998-2018, as revealed by satellite thermal data. Three periodicities emerged from the study: i) long-term ii) intermediate-term, and, iii) short-term.

The long-term periodicity extracted from wavelet analysis is ca. 913-547 days (ca. 1.5-2.5 years). It was replicated by the dual magma chamber model which provided a periodicity of ca. 1000-500 days. The intermediate-term periodicity obtained from wavelet analysis is ca. 146-292 days (ca. 5-10 months), fairly replicated by the single magma chamber model with a periodicity of ca. 220 days. The short-term periodicity of ca. 18-38 days (ca. 2.5-5 weeks) is matched by model outputs considering the dynamics of the upper conduit (ca. 16-40 days). The depicted behaviour of effusive activity at Fuego de Colima is here presented for the first time, showing how the volcano presents

similarities with eruptive dynamics of other recent lava dome eruptions (i.e. SHV, Montserrat, Costa et al., 2013).

Code availability

Melnik and Costa (2014) code is a research software and is not still available for distribution as it lacks of documentation. It can be used by contacting the authors under their supervision.

Data availability

The original thermal dataset is available on www.mirovaweb.it. Excel worksheets can be obtained by contacting the authors.

Appendices

Appendix A1. Sensitivity tests for steady state solutions of discharge rate vs chamber pressure (top) and time evolution of discharge rates (bottom). These solutions are referred to the following main input parameters: i) dyke thickness $2b$ = 40 m as the conduit diameter at the top ($D=2b$), the transition from the dyke to cylindrical conduit L_T = 500 m below the surface, the length of the dyke L_d = 6 km, and the volume of the magma chamber V_{ch} = 50 km^3. (a) General solution showing the transient regime where the periodicity can occur; (b) Solutions influenced by the dyke width $2a$ (from 200 to 400 m); (c) Solutions influenced by the proportion of the water content in the melt (H_2O from 4 to 5 %).

Appendix A2. Sensitivity tests for transient solutions using the single magma chamber model. As a reference these solutions have the same main input parameters used for A1. (a) Dependence of discharge rate on time considering the influence of the dyke width $2a$ (from 200 to 400 m); (b) Influence of the magma chamber volume V_{ch} (from 20 to 50 km^3); (c) Dependence of discharge rate on time considering the dyke elasticity. Each curve shows a solution with a constant influx rate Q_{in} (in the range of 0.01- 0.1 m^3 s^{-1}).

Appendix A3. Sensitivity tests for transient solutions using the dual magma chamber model. The shallow feeding system has dyke with a width $2a$ = 200 m, $2b$ = 40 m, and L_T = 500 m. The cylindrical conduit diameter $D = 2b$. For each diagram, is indicated the outflow (Q_{out}; black red and green lines), the flux entering into the shallower magma chamber (Q_{ins}; blue line) and periods in days (T). Runs of Section 1-2-3 have fixed $Q_{in,d}$ = 2.3 (m^3 s^{-1}).

- *Section 1*) The volumes of the shallow and deep magma chambers are fixed to 40 km^3 and 650 km^3, respectively. A set of runs is carried out for three different aspect ratios (*AR*) of the shallow and deep chambers (*ARs* = 1; *ARd* = 1, *ARs* = 2; *ARd* = 1, *ARs* = 2; *ARd* = 1.5) considering three widths of the deeper dyke ($2a_{0d}$ = 200 m - black line, 1000 m - red line, 3000 m - green line).
- *Section 2*) The volume of the deeper magma chamber and the aspect ratios of both shallow and deep chambers are fixed to 650 km^3 and *ARs* = *ARd* = 1. A set of runs is provided for three different shallow chamber volumes (V_{chs} = 30 km^3, 40 km^3, 50 km^3) considering three widths of the deeper dyke ($2a_{0d}$ = 200 m - black line, 1000 m - red line, 3000 m - green line);
- *Section 3*) The shallow chamber volume and the aspect ratios of both shallow and deep chambers are fixed to 40 km^3 and *ARs* = *ARd* = 1, respectively. A set of runs is carried out for three deep chamber volumes (V_{chd} = 550 km^3, 650 km^3, 750 km^3) considering three widths of the deeper dyke ($2a_{0d}$ = 200 m - black line, 1000 m - red line, 3000 m - green line).
- *Section 4*) The shallow and deep chamber volumes are fixed to 40 km^3 and 650 km^3, respectively. Two set of runs are carried out for $Q_{in,d}$ equal to 1 and 3 (m^3 s^{-1}). The aspect ratios (*AR*) of the shallow and deep chambers are both equal to 1, considering three widths of the deeper dyke ($2a_{0d}$ = 200 m - black line, 1000 m - red line, 3000 m - green line).

Appendix A4. Results of the Fourier analysis. (a) The 2002-2006 period shows two main periodic components, T_0 = 24.70 and T_1 = 6.17 months, corresponding to ca. 2 years and ca. 6 months, respectively; (b) The 2013-2016 period shows similar results: T_0 = 24.94 and T_1 = 6.23 months, corresponding to ca. 2.1 years and ca. 6 months, respectively.

Author's contribution

SM and AC compiled the numerical simulations and formulated the adopted methodology. DC provided and processed the satellite thermal data. LC provided the volcanological data. SM and RS wrote the manuscript with the input of all co-authors. All authors worked on the interpretation of the results.

Competing interests

The authors declare that they have no conflict of interest.

Acknowledgments

SM thanks Centro de Geociencias of Queretaro (UNAM, Mexico) for the hospitality during the period of research at Fuego de Colima volcano, the Doctoral Course in Geoscience of University of Bari (Italy) for the partial financial support, and Dr. F. Loparco for the help with the Python coding. LC was supported by PAPIIT-UNAM n° 105116 project. All authors are grateful to the reviewers for their valuable comments and suggestions useful to improve the manuscript.

References

Aràmbula-Mendoza, R., Lesage, P., Valdèz-Gonzales, C., Varley, N., Reyes-Dàvila, G. and Navarro-Ochoa, C.: Seismic activity that accompagnied the effusive and explosive eruptions during the 2004–2005 period at Volcàn de Colima, Mexico, J. Volcanol. Geotherm. Res., 205, 30–46, 2011.

Arámbula-Mendoza, R., Reyes-Dávila, G., Dulce, M. V. B., González-Amezcua, M., Navarro-Ochoa, C., Martínez-Fierros, A., and Ramírez-Vázquez, A.: Seismic monitoring of effusive-explosive activity and large lava dome collapses during 2013–2015 at Volcán de Colima, Mexico. J. Volcanol. Geotherm. Res., 351, 75-88, 2018.

Barmin, A., Melnik, O. and Sparks, R.S.J.: Periodic behavior in lava dome eruptions, Earth Planet. Sci. Lett., 199 (1), 173-184, 2002.

Belousov, A., Voight, B., Belousova, M. and Petukhin, A.:Pyroclastic surges and flows from the 8-10 May 1997 explosive eruption of Bezymianny volcano, Kamchatka, Russia, B. Volcanol., 64 (7), 455-471, 2002.

Bernstein, M., Pavez, A., Varley, N., Whelley, P. and Calder, E.S.: Rhyolite lava dome growth styles at Chaitén Volcano, Chile (2008-2009): Interpretation of thermal imagery, Andean Geology, 40 (2), 2013.

Brèton-Gonzalez, M., Ramirez, J.J. and Navarro-Ochoa, C.: Summary of the historical eruptive activity of Volcan de Colima, Mexico 1519-2000, J. Volcanol. Geotherm. Res., 117, 21–46, 2002.

Bonasia, R., Capra, L., Costa, A., Macedonio, G., and Saucedo, R.: Tephra fallout hazard assessment for a Plinian eruption scenario at Volcán de Colima (Mexico), J. Volcanol. Geotherm. Res., 203, 12-22, 2011.

Capra, L., Borselli, L., Varley, N., Gavilanes-Ruiz, J. C., Norini, G., Sarocchi, D., and Cortes, A.: Rainfall-triggered lahars at Volcán de Colima, Mexico: surface hydro-repellency as initiation process. J. Volcanol. Geotherm. Res., 189 (1-2), 105-117, 2010.

Capra, L., Macías, J.L., Cortés, A., Dávila, N., Saucedo, R., Osorio-Ocampo, S., Arce, J.L., Galvilanes-Ruiz, J.C., Corona-Càvez, P., Gàrcia-Sancez, L., Sosa-Ceballos, G., Vasquez, R.: Preliminary report on the July 10–11, 2015 eruption at Volcán de Colima: Pyroclastic density currents with exceptional runouts and volume, J. Volcanol. Geotherm. Res., 310,

690 39-49, 2016.

691 Cazelles, B., Chavez, M., Berteaux, D., Ménard, F., Vik, J. O., Jenouvrier, S., and Stenseth, N.C.:
692 Wavelet analysis of ecological time series. Oecologia, 156(2), 287-304, 2008.
693
694 Christopher, T.E., Blundy, J., Cashman, K., Cole, P., Edmonds, M., Smith, P. J., and Stinton, A.:
695 Crustal-scale degassing due to magma system destabilization and magma-gas decoupling
696 at Soufrière Hills Volcano, Montserrat. Geochem. Geophys. Geosyst., 16(9), 2797-2811,
697 2015.

698 Coppola, D., Piscopo, D., Staudacher, T. and Cigolini, C.: Lava discharge rate and effusive
699 pattern at Piton de la Fournaise from MODIS data. J. Volcanol. Geotherm. Res., 184 (1–2),
700 174–192, 2009.

701 Coppola, D., Laiolo, M., Piscopo, D. and Cigolini, C.: Rheological control on the radiant
702 density of active lava flows and domes. J. Volcanol. Geotherm. Res., 249, 39-48, 2013.
703
704 Coppola, D., Laiolo, M., Cigolini, C., Delle Donne, D., and Ripepe, M.: Enhanced volcanic hot-
705 spot detection using MODIS IR data: results from the MIROVA system. Geol. Soc.
706 London, Special Publications, 426(1), 181-205, 2016.
707
708 Costa A. and Macedonio G.: Nonlinear phenomena in fluids with temperature-dependent viscosity:
709 a hysteresis model for magma flow in conduits, Geophys. Res. Lett., 29, 1402, 2002.
710
711 Costa A. and Macedonio, G: Viscous heating in fluids with temperature-dependent viscosity:
712 Triggering of secondary flows, J. Fluid Mech., 540, 21– 38, 2005.
713
714 Costa, A., Melnik, O., Sparks, R.S.J.: Controls of conduit geometry and wallrock elasticity on lava
715 dome eruptions, Earth Planet. Sci. Lett., 260, 137–151, 2007a.
716
717 Costa, A., Melnik, O., Sparks R.S.J. and Voight, B.: Control of magma flow in dykes on
718 cyclic lava dome extrusion, Geophys. Res. Lett., 34 (2), 2007b.
719
720 Costa, A., Melnik, O. and Vedeneeva, E.: Thermal effects during magma ascent in conduits, J.
721 Geophys. Res., Vol. 112, B12205, 2007c.
722
723 Costa A., Caricchi L., Bagdassarov N.: A model for the rheology of particle-bearing
724 suspensions and partially molten rocks, Geochem. Geophys. Geosyst., 10, Q03010,
725 doi:10.1029/2008GC002138, 2009.
726
727 Costa, A., Wadge, G., Melnik, O.: Cyclic extrusion of a lava dome based on a stick-slip
728 mechanism. Earth Planet. Sci. Lett., 337, 39-46, 2012.
729
730 Costa, A., Wadge, G., Stewart, R., Odbert, H.: Coupled subdaily and multiweek cycles during the
731 lava dome eruption of Soufrière Hills Volcano, Montserrat. J. Geophys. Res., Solid Earth,
732 118(5), 1895-1903, 2013.
733
734 Clavijero, F.X.: Historia Antigua de Mexico, Sepan Cuantos, 29, Porrua, 1780.
735
736 Cortés, A., Garduño-Monroy, V.H., Navarro-Ochoa, C., Komorowski, J.C., Saucedo, R., Macías,
737 J.L. and Gavilanes, J.C.: Carta geológica del Complejo Volcánico de Colima, con

738 Geología del Complejo Volcánico de Colima, Univer. Nat. Autón. México, Inst. Geol.,
739 Cartas Geológicas y Mineras, 10, 2005.

740 Daubechies: Ten Lectures on Wavelets. Society for Industrial and Applied Mathematics, 357, 1992.

741 De Bélizal, É., Lavigne, J.C., Gaillard, D. Grancher, I. Pratomo, I., and Komorowski, J.C.: The
742 2007 eruption of Kelut volcano (East Java, Indonesia): phenomenology, crisis
743 management and social response, Geomorphology, 136(1), 165-175, 2012.
744
745 De la Cruz-Reyna, S.: Random patterns of activity of Colima Volcano, Mexico, J. Volcanol.
746 Geotherm. Res., 55, 51–68, 1993.
747
748 Denlinger, R.P. and Hoblitt, R.P.: Cyclic eruptive behavior of silicic volcanoes, Geology, 27 (5),
749 459-462 1999.
750
751 Dragoni, M. and Tallarico, A.: Assumption in the evaluation of lava effusion rates from heat
752 radiation. Geoph. Res. Lett., 36, L08302, 2009.

753 Farge, M.:Wavelet transforms and their applications to tur- bulence. Annu. Rev. Fluid Mech., 24,
754 395–457, 1992.

755 Farquharson, J., Heap, M.J., Varley, N. R., Baud, P. and Reuschlé, T.: Permeability and porosity
756 relationships of edifice-forming andesites: a combined field and laboratory study. J. Volcanol.
757 Geotherm. Res., 297, 52-68, 2015.
758
759 Fougere, P.: On the accuracy of spectrum analysis of red noise processes using maximum entropy
760 and periodogram models: simulation studies and application to geophysical data. J.
761 Geophys. Res. 90, 4355–4366, 1985.

762
763 Garel, F., Kaminski, E., Tait, S., Limare, A.: An experimental study of the surface thermal
764 signature of hot subaerial isoviscous gravity currents: implications for thermal monitoring of
765 lava flows and domes. J. Volcanol. Geotherm. Res.,117, B02205, 2012.

766 Gavilanes-Ruiz, J.C., Cuevas-Muñiz, A., Varley, N., Gwynne, G., Stevenson, J., Saucedo-Girón,
767 R., and Cortés-Cortés, A.: Exploring the factors that influence the perception of risk: The
768 case of Volcán de Colima, Mexico, J. Volcanol. Geotherm. Res., 186(3), 238-252, 2009.
769
770 Global Volcanism Program: Report on Colima (Mexico). In: Wunderman, R (ed.), B. Global
771 Volcanism Net., 23-10, Smithsonian Institution, 1998.
772
773 Global Volcanism Program: Report on Colima (Mexico). In: Wunderman, R (ed.), Bulletin of the
774 Global Volcanism Network, 25-6, Smithsonian Institution, 2000.
775
776 Global Volcanism Program: Report on Colima (Mexico). In: Wunderman, R (ed.), B. Global
777 Volcanism Net., 27-11, Smithsonian Institution, 2002.
778
779 Global Volcanism Program: Report on Colima (Mexico). In: Venzke, E (ed.), B. Global
780 Volcanism Net., 28-11, Smithsonian Institution, 2003.
781
782 Global Volcanism Program: Report on Colima (Mexico). In: Wunderman, R (ed.), B. Global
783 Volcanism Net., 38-12, Smithsonian Institution, 2013.

Global Volcanism Program: Report on Colima (Mexico). In: Sennert, S K (ed.), Weekly Volcanic Activity Report, 26 July-1 August 2017, Smithsonian Institution and US Geological Survey, 2017.

Harris, A.J., Rose, W.I. and Flynn, L.P.: Temporal trends in lava dome extrusion at Santiaguito 1922-2000, B. Volcanol., 65(2), 77-89, 2003.

Harris, A.J.L., Rowland, S.K.: Effusion rate controls on lava flow length and the role of heat loss: a review. In: Thordarson, T., Self, S., Larsen, G., Rowland, S.K., Hoskuldsson, A. (Eds.), Studies in Volcanology: The Legacy of George Walker: Special Publication IAVCEI, 2, pp. 33–51, 2009.

Harris, A.J.L., Favalli, M., Steffke, A., Fornaciai, A., Boschi, E.:A relation between lava discharge rate, thermal insulation, and flow area set using lidar data. Geoph. Res. Lett., 37, L20308. http://dx.doi.org/10.1029/2010GL044683, 2010.

Heap, M.J., Lavallée, Y., Petrakova, L., Baud, P., Reuschle, T., Varley, N., and Dingwell D.B.: Microstructural controls on the physical and mechanical properties of edifice-forming andesites at Volcán de Colima, Mexico, Solid Earth, 119 (4), 2925-2963, 2014.

Hutchison, W., Varley, N., Pyle, D.M., Mather, T.A., and Stevenson, J.A.: Airborne thermal remote sensing of the Volcán de Colima (Mexico) lava dome from 2007 to 2010, Geol. Soc. London, Spec. Public., 380 (1), 203-228, 2013.

James, M. R. and Varley, N.: Identification of structural controls in an active lava dome with high resolution DEMs: Volcán de Colima, Mexico. Geoph. Res.Lett., 39(22), 2012.

Kavanagh, J. L. and Sparks, R.S.J.: Insights of dyke emplacement mechanics from detailed 3D dyke thickness datasets. J.Geol. Soc., 168(4), 965-978, 2011.

Kozono, T. and Koyaguchi, T.: Effects of relative motion between gas and liquid on 1-dimensional steady flow in silicic volcanic conduits: 2. Origin of diversity of eruption styles. J. Volcanol. Geotherm. Res, 180(1), 37-49, 2009.

Kozono, T. and Koyaguchi, T.: Effects of gas escape and crystallization on the complexity of conduit flow dynamics during lava dome eruptions. Geoph. Res.Lett., Solid Earth, 117(B8), 2012.

Lamb, O.D., Varley, N., Mather, T.A., Pyle, D.M., Smith, P.J. and Liu, E.J.: Multiple timescales of cyclical behaviour observed at two dome-forming eruptions, J. Volcanol. Geotherm. Res., 284, 106-121, 2014.

Lau K.M. and Weng H.: Climatic signal detection using wavelet transform: how to make a time series sing. Bull Am Meteorol Soc., 76. 2391–2402, 1995.

Lavallée, Y., Varley, N., Alatorre-Ibargüengoitia, M.A., Hess, K.U., Kueppers, U., Mueller, S., Richard, D., Scheu, B., Spieler, O. and D.B. Dingwell, D.B.: Magmatic architecture of dome-building eruptions at Volcan de Colima (Mexico), Bull. Volcanol., 74 (1), 249-260, 2012.

Lensky, N.G., Navon, O. and Lyakhovsky, V.: Bubble growth during decompression of magma: experimental and theoretical investigation, J. Volcanol. Geotherm. Res., 129 (1), 7-22, 2004.

Loughlin, S.C., Luckett, R., Ryan, G., Christopher, T., Hards, V., De Angelis, S. and Strutt, M.: An overview of lava dome evolution, dome collapse and cyclicity at Soufrière Hills Volcano, Montserrat, 2005–2007, Geophys. Res. Lett., 37 (19), 2010.

Luhr, J.F. and Carmichael, I.S.: The Colima Volcanic Complex, Mexico, Con.to Mineral.Petrol., 71 (4), 343-372, 1980.

Luhr, J.F.: Petrology and geochemistry of the 1991 and 1998-1999 lava flows from Volcan Colima, Mexico, J. Volcanol. Geotherm. Res., 117, 169–194, 2002.

Macìas, J., Arce, J., Sosa, G., Gardner, J.E., Saucedo, R.:Storage conditions and magma processes triggering the 1818CE Plinian eruption of Volcán de Colima, J. Volcanol. Geotherm. Res., doi:10.1016/j.jvolgeores.2017.02.025, 2017.

Mallat, S.: A wavelet tour of signal processing. Academic Press, San Diego, 1998.

Massaro, S., Sulpizio, R.,Costa, A., Capra, L., Lucchi, F.: Understanding eruptive style variations at calc-alkaline volcanoes: the 1913 eruption of Fuego de Colima volcano (Mexico), B. Volcanol, 80-62, https://doi.org/10.1007/s00445-018-1235-z, 2018a.

Massaro, S., Costa, A., Sulpizio, R.: Time evolution of a magma feeding system during a Plinian eruption: the example of the Pomici di Avellino eruption of Somma-Vesuvius (Italy), Earth Planet. Sci. Lett. 482, 545-555, 2018b.

Medina-Martinez, F.: Analysis of the eruptive history of the Volcán de Colima, Mexico (1560–1980), Geofisica Internacional, 22, 157–178, 1983.

Martin del Pozzo, A.L., Sheridan, M., Barrera, D., Lugo Hubp, J. and Vázquez Selem, L.: Potential hazards from Colima volcano, Mexico, Geofisica Internacional, 34 (4), 363-376. 1995.

Melnik, O. and Sparks, R.S.J.: Nonlinear dynamics of lava dome extrusion, Nature, 402 (6757), 37-41, 1999.

Melnik, O. and Sparks, R.S.J: Dynamics of magma ascent and lava extrusion at Soufrière Hills Volcano, Montserrat, Geol. Soc. London Mem., 21 (1), 153-171, 2002.

Melnik, O. and Sparks, R.S.J: Controls on conduit magma flow dynamics during lava-dome building eruptions, J. Geophys. Res., 110, B02209, doi:10.1029/2004JB003183, 2005.

Melnik, O., Sparks, R.S.J., Costa, A. and Barmin, A.: (2008), Volcanic Eruptions: Cyclicity during Lava Dome Growth, in Meyers: Encyclopedia of Complexity and Systems Science, 2008.

Melnik, O. and A. Costa, A: Dual-chamber-conduit models of non-linear dynamics behaviour at Soufrière Hills Volcano, Montserrat, Geol. Soc. Lond., Mem., 39, 61-69, 2014.

877 Mériaux, C. and Jaupart, C: Simple fluid dynamic models of volcanic rift zones, Earth Planet. Sci.
878 Lett., 136(3-4), 223-240, 1995.
879
880 Mora, J. C., Macıas, J. L., Saucedo, R., Orlando, A., Manetti, P., and Vaselli, O.: Petrology of the
881 1998–2000 products of Volcán de Colima, México. J. Volcanol. Geotherm. Res., 117(1),
882 195-212, 2002.
883
884 Mueller, S.B., Varley, N., Kueppers, U., Lesage, P. and Reyes-Dàvila, G.: Quantification of
885 magma ascent rate through rockfall monitoring at the growing/collapsing lava dome of
886 Volcan de Colima, Mexico, Solid Earth, 4, 201-213, 2013.
887
888 Nakanishi, M. and Koyaguchi, T.: A stability analysis of a conduit flow model for lava dome
889 eruptions. J. Volcanol. Geotherm. Res., 178(1), 46-57, 2008.
890
891 Nakada, S., Shimizu, H. and Ohta, K.: Overview of the 1990–1995 eruption at Unzen Volcano, J.
892 Volcanol. Geotherm. Res., 89 (1), 1-22, 1999.
893
894 Navarro-Ochoa, C., Gavilanes-Ruiz, A. Cortès-Cortès, A.: Movement and emplacement of lava
895 flows at Volcán de Colima, México: November 1998–February 1999, J. Volcanol.
896 Geotherm. Res., 117 (1), 155-167, 2002.

897 Nicholson, R.S., Gardner, J.E., and Neal, C.A.: Variations in eruption style during the 1931 A.D.
898 eruption of Aniakchak volcano, Alaska, J. Volcanol. Geotherm. Res., 207, 69–82, 2011.

899 Norini, G., Capra, L.,Groppelli, G., Agliardi, F., Pola, A., and Cortès, A.: Structural architecture of
900 the Colima Volcanic Complex, J. Geophys. Res., 115, B12209, 2010.
901
902 Odbert, H.M. and Wadge, G.: Time series analysis of lava flux. J. Volcanol. Geotherm. Res.,
903 188(4), 305-314, 2009.
904
905 Ozerov, A., Ispolatov, I. and Lees, J.: Modeling strombolian eruptions of Karymsky volcano,
906 Kamchatka, Russia, J. Volcanol. Geotherm. Res.,122 (3), 265-280, 2003.
907
908 Ramsey, M.S. and Harris, A.J.L.:Volcanology 2020: how will thermal remote sensing of
909 volcanic surface activity evolve over the next decade? J. Volcanol. Geotherm. Res.,
910 http://dx.doi.org/10.1016/j.jvolgeores.2012.05.011, 2012.

911 Reyes-Dávila, G.A., Arámbula-Mendoza, R., Espinasa-Pereña, P., Pankhurst, M.J., Navarro-
912 Ochoa, C., Savov, I. and Domínguez-Reyes, T.: Volcán de Colima dome collapse of
913 July, 2015 and associated pyroclastic density currents, J. Volcanol. Geotherm. Res, 320,
914 100-106, 2016.
915
916 Reubi, O. and Blundy. J: Assimilation of Plutonic roots, formation of high-K exotic melt
917 inclusions and genesis of andesitic magmas at Volcán De Colima, Mexico, J. Petrol. 49, 12,
918 2221–2243, 2008.
919
920 Reubi, O., Blundy, J. and Varley, N.: Volatiles contents, degassing and crystallisation of
921 intermediate magmas at Volcán de Colima, Mexico, inferred from melt inclusions.
922 Contr. Mineral. Petrol., 165(6), 1087-1106, 2013.

Reubi, O., Sims, K.W., Varley, N., Reagan, M. and Eikenberg, J.: Timescales of degassing and conduit dynamics inferred from 210Pb–226Ra disequilibria in Vòlcan de Colima 1998–2010 andesitic magmas. Geol. Soc., London, Sp. Publ., 422, SP422-5, 2015.

Roverato, M., Capra, L., Sulpizio, R., Norini, G.: Stratigraphic reconstruction of two debris avalanche deposits at Colima Volcano (Mexico): insights into pre-failure conditions and climate influence. Journal of Volcanology and Geothermal Research, 207(1-2), 33-46, 2011.

Salzer, J.T., Nikkhoo, M., Walter, T.R., Sudhaus, H., Reyes-Dávila, G., Bretón, M. and Arámbula, R.: Satellite radar data reveal short-term pre-explosive displacements and a complex conduit system at Volcán de Colima, Mexico, Frontiers in Earth Sci., 2, 12, 2014.

Saucedo, R., Macìas, J.L., Sheridan, M.F., Bursik, M.I., Komorowski, J.C.: Modeling of pyroclastic flows of Colima Volcano, Mexico: implications for hazard assessment, J. Volcanol. Geotherm. Res., 139 (1–2), 103–115, 2005.

Saucedo, R., J.L. Macías, J.C. Gavilanes, J.L. Arce, J.C. Komorowski, J.E. Gardner, and G. Valdez-Moreno, G.: Eyewitness, stratigraphy, chemistry, and eruptive dynamics of the 1913 Plinian eruption of Volcán de Colima, México, J. Volcanol. Geotherm. Res., 191(3), 149-166, 2010.

Savov, I.P., Luhr, J.F. and Navarro-Ochoa, C.; Petrology and geochemistry of lava and ash erupted from Volcan Colima, Mexico, during 1998-2005, J. Volcanol. Geotherm. Res., 174, 241–256, 2008.

Siswowidjoyo, S., Suryo, I. and Yokoyama, I.: Magma eruption rates of Merapi volcano, Central Java, Indonesia during one century (1890–1992), B. Volcanol., 57 (2), 111-116, 1995.

Sparks, R.S.J.:Causes and consequences of pressurisation in lava dome eruptions, Earth Planet. Sci. Lett., 150 (3-4), 177-189, 1997.

Sparks, R.S.J. and Young, S.R.: The eruption of Soufrière Hills volcano, Montserrat (1995–1999): Overview of scientific results, in The Eruption of the Soufrière Hills Volcano, Montserrat from 1995 to 1999, Geol. Soc. London Mem., 21, 45– 69, 2002.

Spica, Z., Perton, M. and Legrand, D.: Anatomy of the Colima volcano magmatic system, Mexico, Earth Planet. Sci. Lett., 459, 1-13, 2017.

Sulpizio, R., Capra, L., Sarocchi, D., Saucedo, R., Gavilanes-Ruiz, J. C. and Varley, N.: Predicting the block-and-ash flow inundation areas at Volcán de Colima (Colima, Mexico) based on the present day (February 2010) status. J. Volcanol. Geotherm. Res., 193(1-2), 49-66, 2010.

Swanson, D.A. and Holcomb, R.T.: Regularities in growth of the Mount St. Helens dacite dome, 1980–1986, in Lava Flows and Domes: Emplacement Mechanisms and Hazard Implications, 3-24, 1990.

Thiele, S.T., Varley, N. and James, M.R.: Thermal photogrammetric imaging: A new technique for monitoring dome eruptions, J. Volcanol. Geotherm. Res., 337, 140-145, 2017.

Trauth, M.: MATLAB Recipes for Earth Sciences, 1st ed. Springer-Verlag, Berlin Heidelberg, 2006.

975 Torrence, C. and Compo, G.P.:A practical guide to wavelet analysis. Bulletin of the American
976 Meteorological society, 79(1), 61-78, 1998.
977
978 Varley, N., Arámbula-Mendoza, R., Reyes-Dávila, G., Stevenson, J., Harwood, R.: Long-
979 period seismicity during magma movement at Volcán de Colima, B. Volcanol,. 72, 1093–
980 1107. http://dx.doi.org/10.1007/s00445-010-0390-7, 2010a.
981
982 Varley, N., Aràmbula-Mendoza, R., Reyes-Reyes-Dàvila, G., Sanderson, R., Stevenson, J.:
983 Generation of Vulcanian activity and long-period seismicity at Volcan de Colima, Mexico.
984 J. Volcanol. Geotherm. Res., 198, 45–56, 2010b.

985 Varley, N: La evolución de la actividad reciente del Volcán de Colima, webseminar, Unión
986 Geofísica Mexicana A.C., 2015.
987
988 Vila, J., Macià, R., Kumar, D., Ortiz, R., Moreno, H., Correig, A.: Analysis of the unrest of active
989 volcanoes using variations of the base level noise seismic spectrum. J. Volcanol. Geotherm.
990 Res. 153, 11–20, 2006.

991 Voight, B., Hoblitt, R.P., Clarke, A.B., Lockhart, A. Miller, L. Lynch and McMahon, J.:
992 Remarkable cyclic ground deformation monitored in real-time on Montserrat, and its use
993 in eruption forecasting, Geophys. Res. Lett., 25 (18), 3405-3408, 1998.
994
995 Voight, B.,.Sparks, R.S.J., Miller, A.D., Stewart, R.C., Hoblitt, R.P., Clarke, A. and Cole, P.:
996 Magma flow instability and cyclic activity at Soufriere Hills volcano, Montserrat,
997 british west indies, Science, 283 (5405), 1138-1142, 1999.
998
999 Voight, B., Constantine, E.K., Siswowidjoyo, S. and Torley, R.: Historical eruptions of Merapi
1000 volcano, central Java, Indonesia, 1768–1998, J. Volcanol. Geotherm. Res., 100 (1), 69-138,
1001 2000.
1002
1003 Wadge, G., Dorta, D.O. and Cole, P.D.: The magma budget of Volcán Arenal, Costa Rica
1004 from 1980 to 2004, J. Volcanol. Geotherm. Res., 157 (1), 60-74, 2006.
1005
1006 Wadge, G., Herd, R., Ryan, G.,Calder, E.S. and Komorowski, J.C.: Lava production at Soufrière
1007 Hills Volcano, Montserrat: 1995–2009, Geophys. Res. Lett., 37 (19), 2010.
1008
1009 Watts, R.B., Herd, R.A., Sparks, R.S.J. and Young, S.R.: Growth patterns and emplacementof the
1010 andesitic lava dome at Soufriere Hills Volcano, Montserrat, Geol. Soc. Lond. Mem. 21(1),
1011 115-152, 2002.
1012
1013 Weng, H. and Lau, K.M.: Wavelets, period doubling, and time-frequency localization with
1014 application to organization of convection over the tropical western Pacific. J. Atmos. Sci.,
1015 51, 2523–2541, 1994.

1016 Wolpert, R., Ogburn, L. and Calder, E.S.: The longevity of lava dome eruptions. Journal of
1017 Geophysical Research: Solid Earth, 121(2), 676-686, 2016.
1018
1019 Wylie, J.J., Voight, B. and Whitehead, J.A.: Instability of magma flow from volatile dependent
1020 viscosity, Science, 285, 1883–1885 1999.

Zobin, V.M., Orozco-Rojas, J., Reyes-Dávila, G.A. and Navarro-Ochoa, C.: Seismicity of an andesitic volcano during block-lava effusion: Volcán de Colima, México, November 1998–January 1999, Bull. Volcanol. 67 (7), 679-688, 2005.

Zobin, V.M., Varley, N., González, M., Orozco, J., Reyes, G.A., Navarro-Ochoa, C. and M. Bretón: Monitoring the 2004 andesitic block-lava extrusion at Volcán de Colima, México from seismic activity and SO_2 emission, J. Volcanol. Geotherm. Res., 177 (2), 367-377, 2008.

Zobin, V.M., R. Arámbula, R., Bretón, M., Reyes, G., I. Plascencia, I., Navarro-Ochoa, C. and Martínez, A.: Dynamics of the January 2013–June 2014 explosive-effusive episode in the eruption of Volcán de Colima, México: insights from seismic and video monitoring, Bull. Volcanol. 77(4), 31, 2015.

Tables

Table 1: Input parameters used in numerical simulations.

Notation	Description	Value
c_o	Concentration of dissolved gas (wt.%)	5-6
C_f	Solubility coefficient ($Pa^{-1/2}$)	4.1×10^{-6}
C_m	Specific heat ($J\ kg^{-1}\ K^{-1}$)	1.2×10^{3}
I_0	Max nucleation rate ($m^{-3}\ s^{-1}$)	3×10^{10}
L_*	Latent heat of crystallization ($J\ kg^{-1}$)	3.5×10^{5}
μ_g	Gas viscosity (Pa s)	1.5×10^{-5}
ρ_m	Density of the melt phase ($kg\ m^{-3}$)	2300-2500
ρ_c	Density of the crystal ($kg\ m^{-3}$)	2700-2800
T_{ch}	Magma chamber temperature (K)	1150
P_{ch}	Magma chamber pressure (MPa)	130 – 210
β_{ch*}	Magma chamber crystal content	0.35-0.45
μ	Magma viscosity (Pa s)	3.7×10^{5}
ρ_r	Host rock density ($kg\ m^{-3}$)	2600
G	Host rock rigidity (GPa)	6
ν	Poisson's ratio	0.25
ε		8.6

Conduit geometry parameters using a single magma chamber model

D	Diameter of the cylindrical conduit	30-40
L_T	Dyke-cylinder transition depth (m)	1300-500
$2a$	Dyke width (m)	200 – 600
$2b$	Dyke thickness (m)	4-40
L	Magma chamber depth (top) (m)	6000-6500
V_{ch}	Magma chamber volume (km^3)	20-50
AR	Magma chamber aspect ratio	1-2
$Q_{in,s}$	Influx into the shallow magma chamber ($m^3\ s^{-1}$)	0.01-3.5

Parameters used for simulations carried out with dual magma chamber model

Deep magma chamber

$2a_{0d}$	Deeper dyke width (m)	200 – 3000
L_0	Deep magma chamber depth (top) (m)	15000
ARd	Deep magma chamber aspect ratio	1-2
V_{chd}	Deep magma chamber volume (km^3)	550-750
ΔP	Deep magma chamber overpressure (MPa)	20
$Q_{in,d}$	Influx into the shallow magma chamber ($m^3 s^{-1}$)	1-3

Figures Captions

Fig. 1. (a) Digital elevation model of the Colima Volcanic Complex (NC = Nevado de Colima volcano; FC = Fuego de Colima volcano) and Colima Rift with the main tectonic and volcano-tectonic structures (modified from Norini et al. 2010). In the inset, the location of the Colima Volcanic Complex (CVC) within the Trans-Mexican Volcanic Belt (TMVB) is shown in the frame of the subduction-type geodynamic setting of Central America. (b) Schematic view of the conduit feeding system framework used for numerical simulations (modified after Melnik and Costa, 2014).

Fig. 2. Dataset about the averaged discharge rates of Fuego de Colima during 1998-2018, derived by the MIROVA thermal data (black points) and published data (blue crosses) (Navarro-Ochoa et al., 2002; Zobin et al., 2005; Reubi et al 2013; Mueller et al., 2013; Varley, 2015; Reyes-Dàvila et al., 2016; Thiele et al., 2017; GVP, 2002-2017). Values > 0.1 ($m^3\ s^{-1}$) are considered to be as "high" (dark blue area) and values < 0.1 ($m^3\ s^{-1}$) as "low" discharge rate (light blue area). The 0.01 ($m^3\ s^{-1}$) is the threshold under which the MIROVA system does not provide reliable data (blue line); (a) Weekly average discharge rates. The boxes contain symbols of volcanological observations reported in literature; (b) Monthly average discharge rates; (c) Yearly average discharge rates.

Fig. 3. (a) Local wavelet power spectrum normalized by $1/\sigma^2$ (σ^2 in $(m^3\ s^{-1})^2$). The left axis is the period (in years). The bottom axis is time (in years). The shaded contours are at normalized variances of 0.5, 1, 2, and 4 $(m^3\ s^{-1})^2$). The black thick contour encloses regions of greater than 95% confidence for a red-noise process with a lag-1 coefficient of 0.72. It shows three orders of periodicities of: long-term (ca. 1.5-2.5 years), intermediate-term (ca. 5-10 months) during 2002-2006 and 2013-2016, and short-term (ca. 2.5-5 weeks) during 2001-2006 and 2011-2016. Blue line indicates the "cone of influence" where edge effects become important outside it; (b) Global wavelet power spectrum. The green dotted line represents the best-fitting red noise spectrum at the 95% confidence level.

Fig. 4. Results of numerical simulations. The physical framework of the conduit feeding system has deep and shallow chambers connected to surface via vertical elastic dykes evolving into non-elastic cylinder. The length of the shallow dyke L_{ds} is in the range of 6000-6500 m. The passage to cylinder conduit L_T occurs at ca. 1300-500 m below the cone. (a) Discharge rates vs. time considering the elasticity of the shallower dyke, with a width $2a$ = 400 m and thickness $2b$ = 2 m. The cylinder diameter D = 30 m. Two cases are shown: *i)* constant pressure (blue line) and *ii)* constant influx rate at the source region of the dyke, providing different periodicities of 16 and 40 days, in good agreement with the short-term (weekly) periodicities observed in Fig. 3a; (b) Discharge rate vs. time using the single magma chamber model. The dyke width $2a$ = 600 and thickness $2b$ = 4 m. The chamber has a volume V_{ch} = 30 km^3, receiving a constant influx $Q_{in,s}$ = 2.3 $(m^3\ s^{-1})$; Periodicity is of ca. 220 days, in good agreement with the intermediate-term (monthly) periodicities observed in Fig. 3a; (c) Discharge rate vs. time using the dual magma chamber model. The aspect ratio of the shallow and deep chambers (*ARs* - *ARd*) are both equal to 1.3 and 1.4, respectively. The upper feeding system has a chamber (V_{chs} =30 km^3) connected to a dyke (width $2a$ = 260 m; $2b$ = 4 m) evolving into a cylinder (D = 30 m) at L_T = 1000 m. The shallow chamber is connected to the deep one (V_{chd} = 500 km^3) through a feeder dyke ($2a_{0d}$ = 500 m). A constant $Q_{in,d}$ = 2.3 $(m^3\ s^{-1})$ is injected from below. Periodicity is in the range of ca. 825 days, in good agreement with the long-term (yearly) periodicities observed in Fig. 3a.

Fig.1

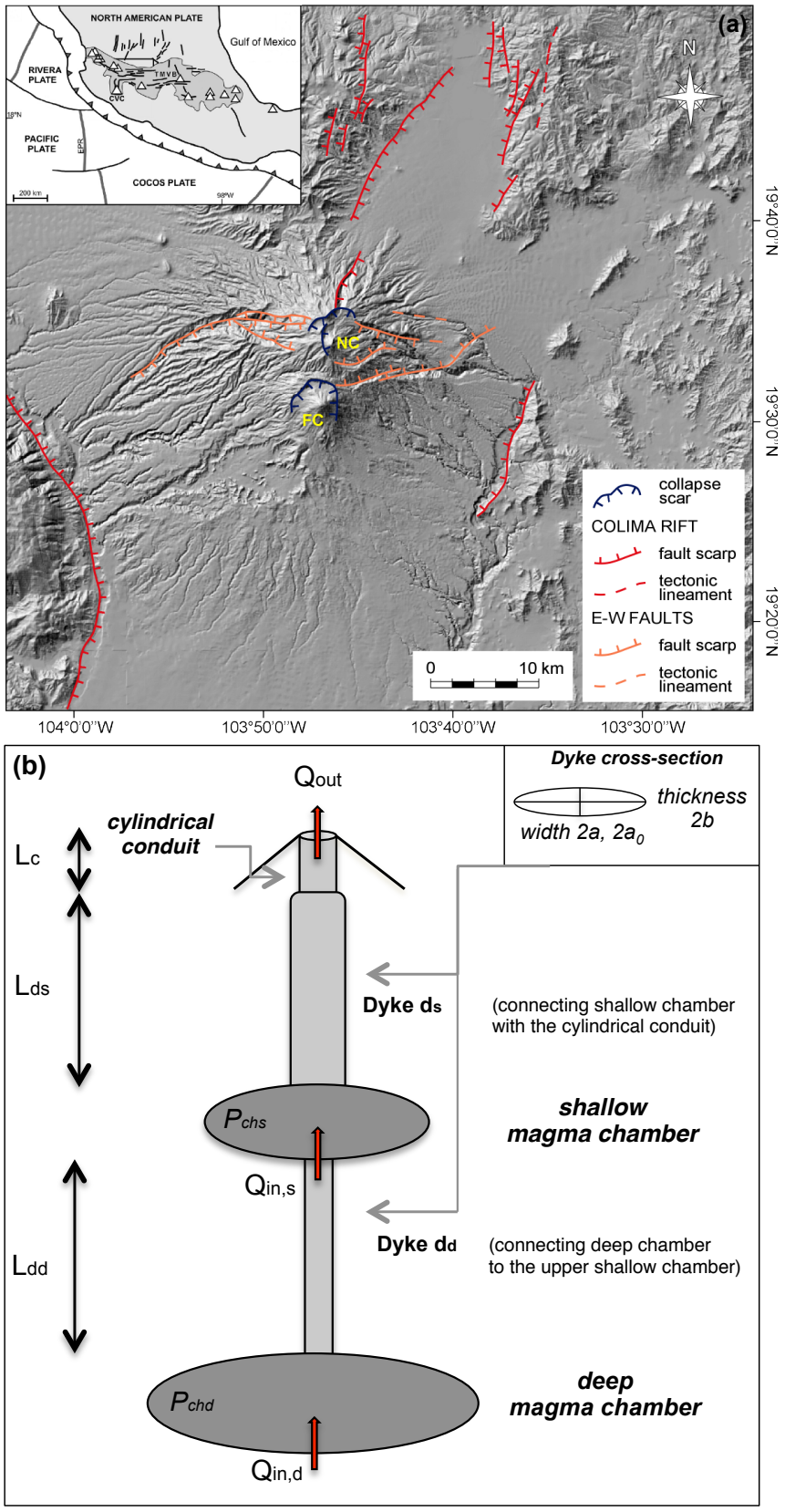
(a)
NORTH AMERICAN PLATE
Gulf of Mexico
RIVERA PLATE
PACIFIC PLATE
COCOS PLATE
TMVB
CVC
EPR
200 km
98°W
N
NC
FC
collapse scar
COLIMA RIFT
fault scarp
tectonic lineament
E-W FAULTS
fault scarp
tectonic lineament
0
10 km
19°40'0"N
19°30'0"N
19°20'0"N
104°0'0"W
103°50'0"W
103°40'0"W
103°30'0"W
(b)
Dyke cross-section
thickness 2b
width 2a, 2a0
Qout
cylindrical conduit
Lc
Lds
Dyke ds
(connecting shallow chamber with the cylindrical conduit)
Pchs
shallow magma chamber
Qin,s
Dyke dd
(connecting deep chamber to the upper shallow chamber)
Ldd
Pchd
deep magma chamber
Qin,d

105

106 **Fig. 2**

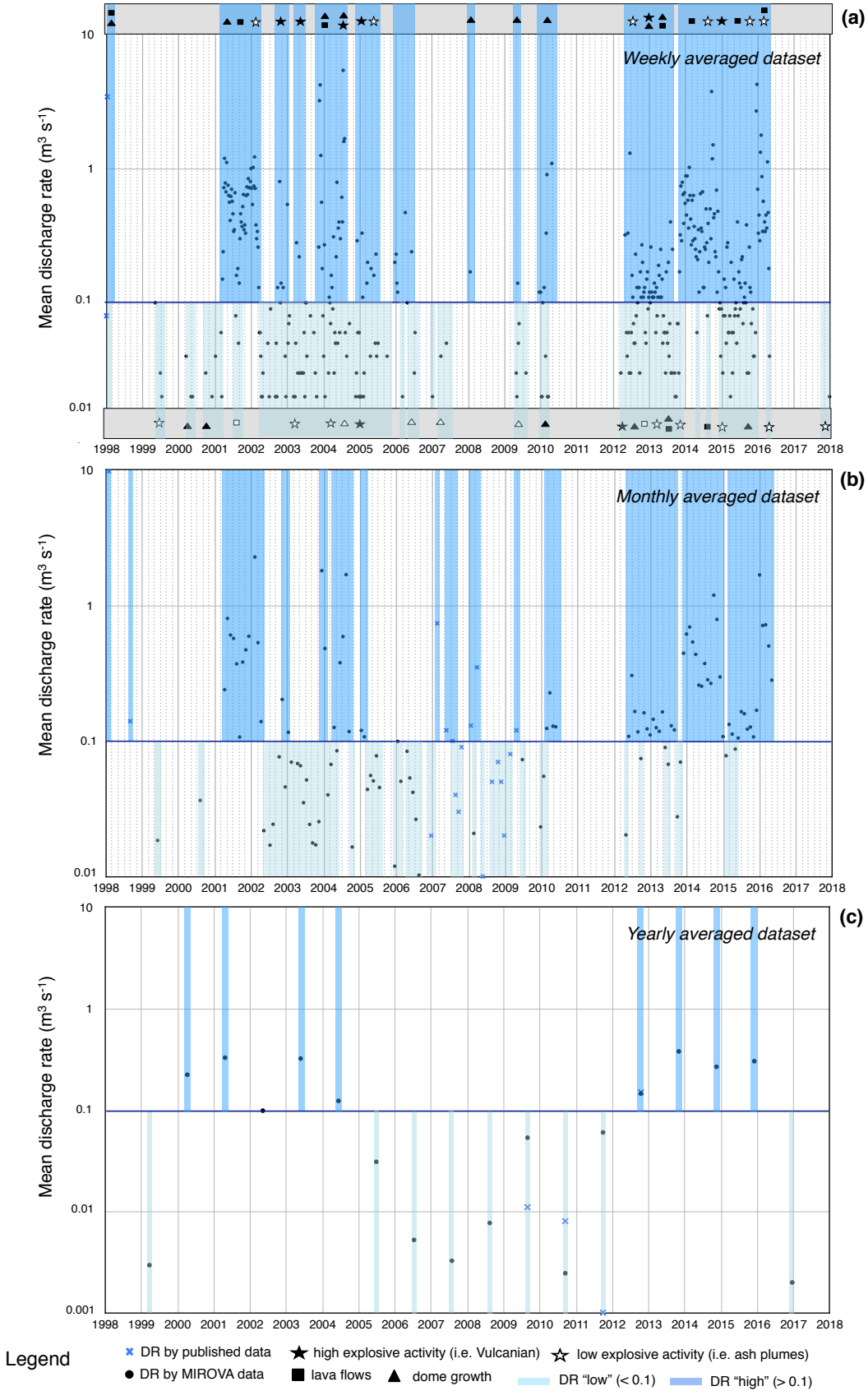
(a)
Weekly averaged dataset
Mean discharge rate (m³ s⁻¹)
10
1
0.1
0.01
1998 1999 2000 2001 2002 2003 2004 2005 2006 2007 2008 2009 2010 2011 2012 2013 2014 2015 2016 2017 2018
(b)
Monthly averaged dataset
Mean discharge rate (m³ s⁻¹)
10
1
0.1
0.01
1998 1999 2000 2001 2002 2003 2004 2005 2006 2007 2008 2009 2010 2011 2012 2013 2014 2015 2016 2017 2018
(c)
Yearly averaged dataset
Mean discharge rate (m³ s⁻¹)
10
1
0.1
0.01
0.001
1998 1999 2000 2001 2002 2003 2004 2005 2006 2007 2008 2009 2010 2011 2012 2013 2014 2015 2016 2017 2018
Legend
DR by published data
high explosive activity (i.e. Vulcanian)
low explosive activity (i.e. ash plumes)
DR by MIROVA data
lava flows
dome growth
DR "low" (< 0.1)
DR "high" (> 0.1)

107

108

109

Fig.3

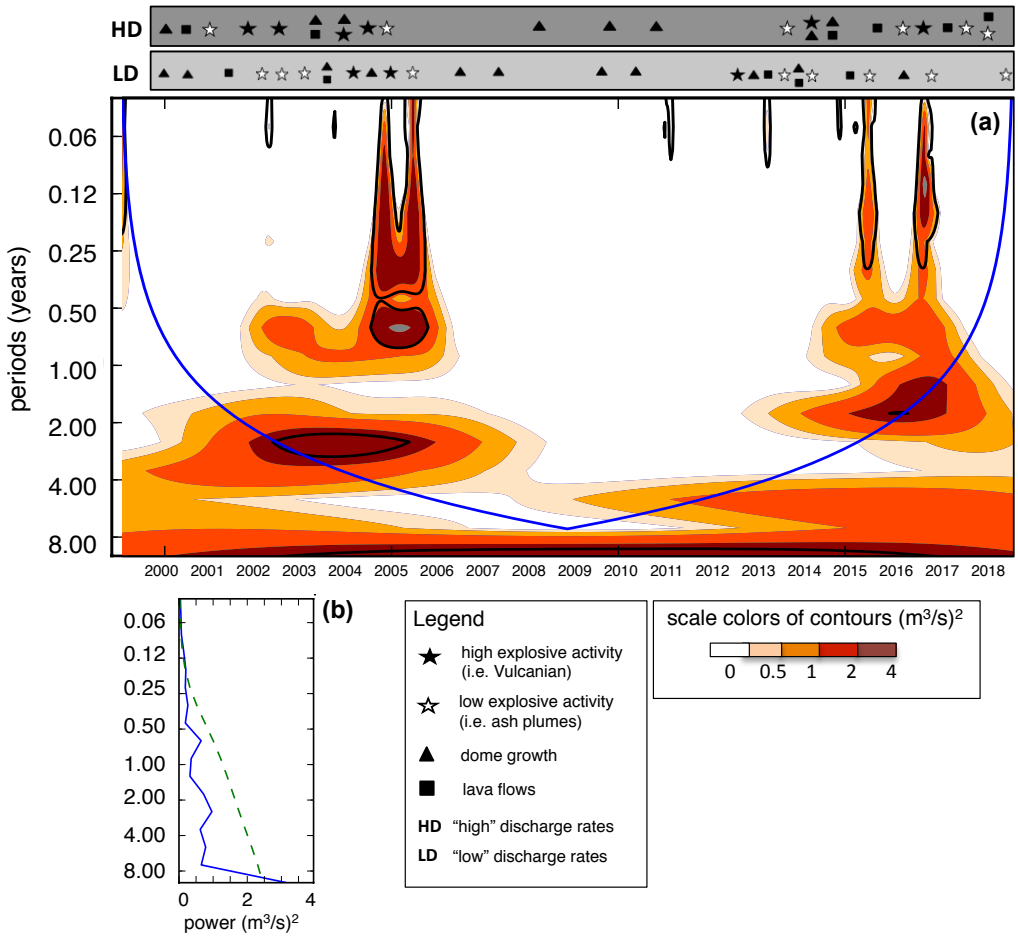
HD
LD
(a)
periods (years)
0.06
0.12
0.25
0.50
1.00
2.00
4.00
8.00
2000 2001 2002 2003 2004 2005 2006 2007 2008 2009 2010 2011 2012 2013 2014 2015 2016 2017 2018
(b)
power (m³/s)²
0 2 4
Legend
high explosive activity (i.e. Vulcanian)
low explosive activity (i.e. ash plumes)
dome growth
lava flows
HD "high" discharge rates
LD "low" discharge rates
scale colors of contours (m³/s)²
0 0.5 1 2 4

Fig. 4

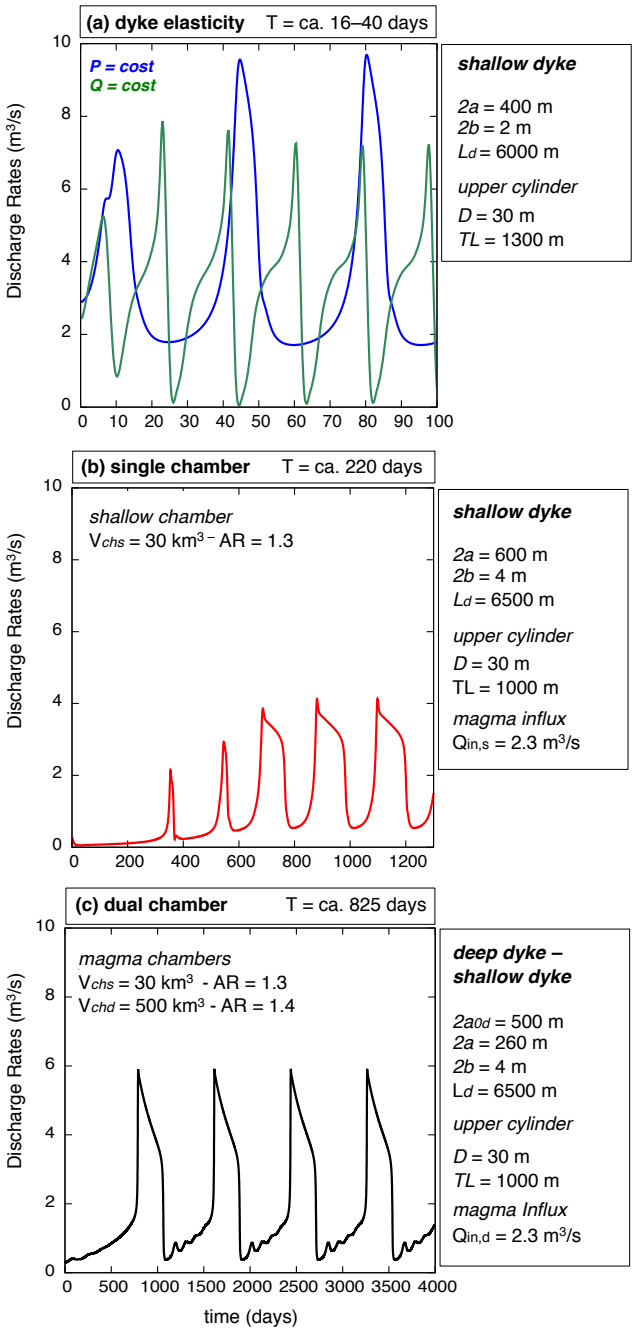
(a) dyke elasticity T = ca. 16–40 days
P = cost
Q = cost
Discharge Rates (m³/s)
shallow dyke
2a = 400 m
2b = 2 m
Ld = 6000 m
upper cylinder
D = 30 m
TL = 1300 m
(b) single chamber T = ca. 220 days
shallow chamber
Vchs = 30 km³ - AR = 1.3
shallow dyke
2a = 600 m
2b = 4 m
Ld = 6500 m
upper cylinder
D = 30 m
TL = 1000 m
magma influx
Qin,s = 2.3 m³/s
(c) dual chamber T = ca. 825 days
magma chambers
Vchs = 30 km³ - AR = 1.3
Vchd = 500 km³ - AR = 1.4
deep dyke – shallow dyke
2a0d = 500 m
2a = 260 m
2b = 4 m
Ld = 6500 m
upper cylinder
D = 30 m
TL = 1000 m
magma Influx
Qin,d = 2.3 m³/s
time (days)

Appendix A1-A2

A1

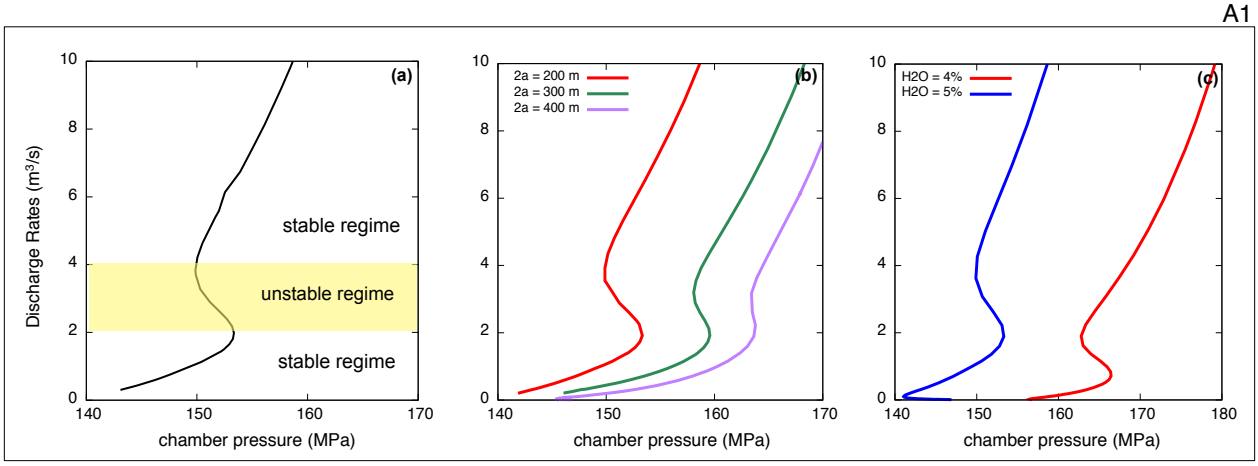

A2

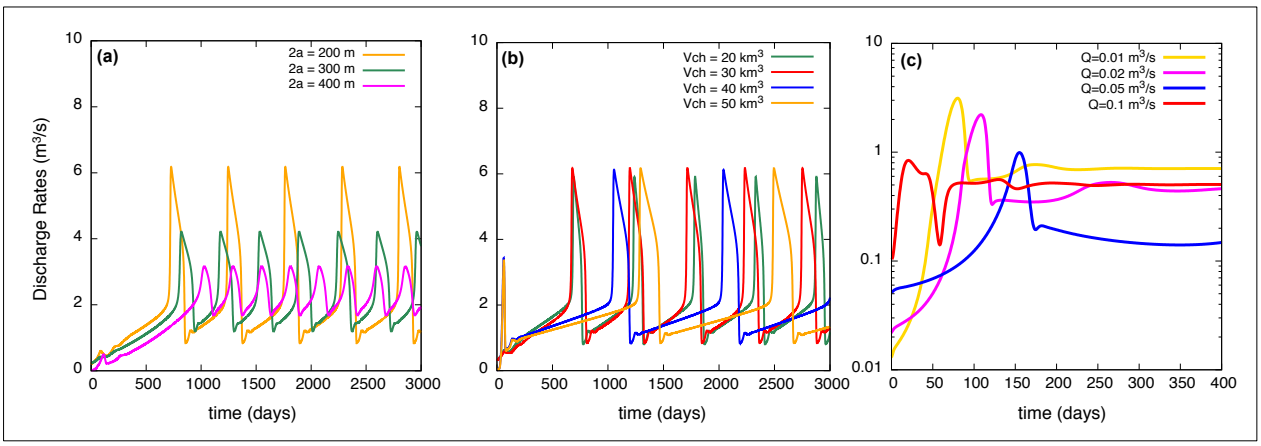

Appendix A3

Fixed parameters
V_{chs} = 40 km³
V_{chd} = 650 km³

Aspect Ratio
ARs = 1
ARd = 1

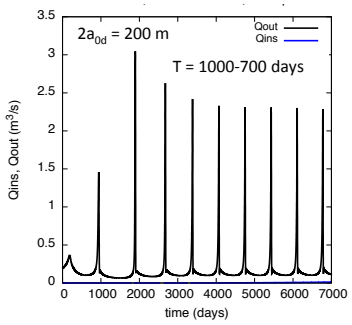

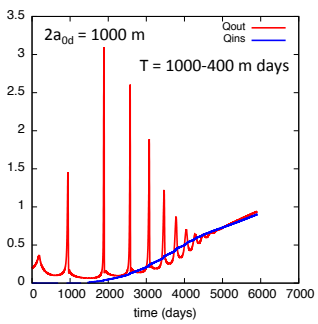

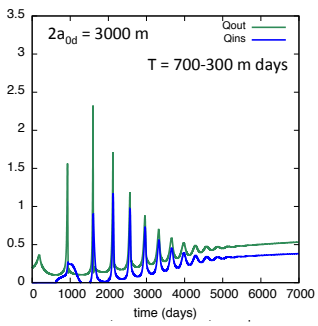

Aspect Ratio
ARs = 2
ARd = 1

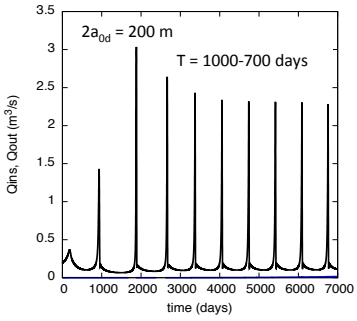

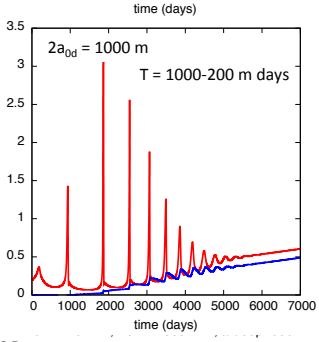

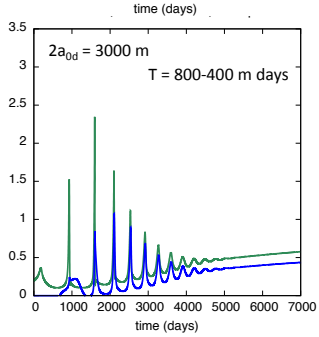

Aspect Ratio
ARs = 2
ARd = 1.5

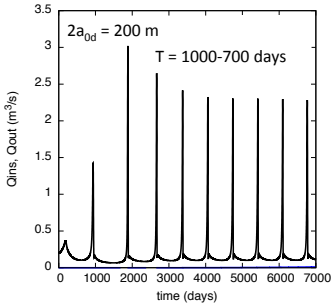

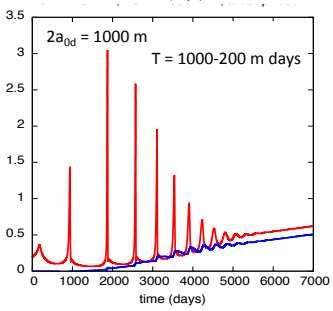

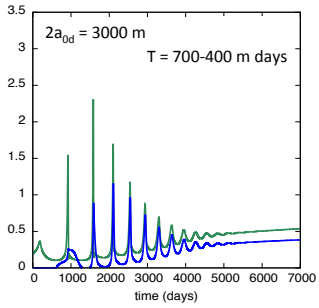

Fixed parameters
ARs = 1
ARd = 1
V_{chd} = 650 km^3

Shallow Chamber Volume

V_{chs} = 30 km^3

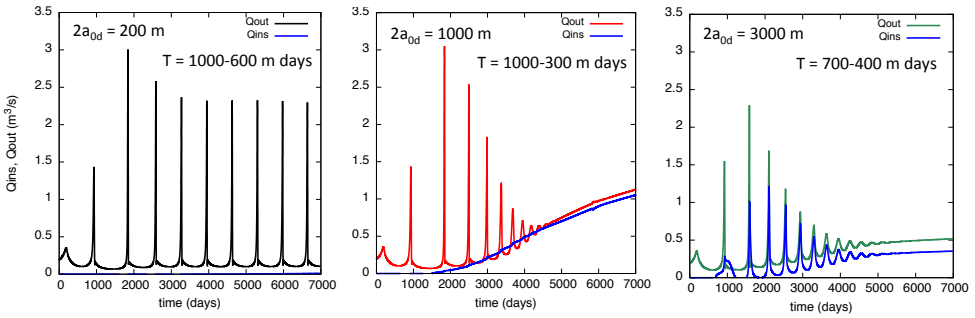

Shallow Chamber Volume

V_{chs} = 40 km^3

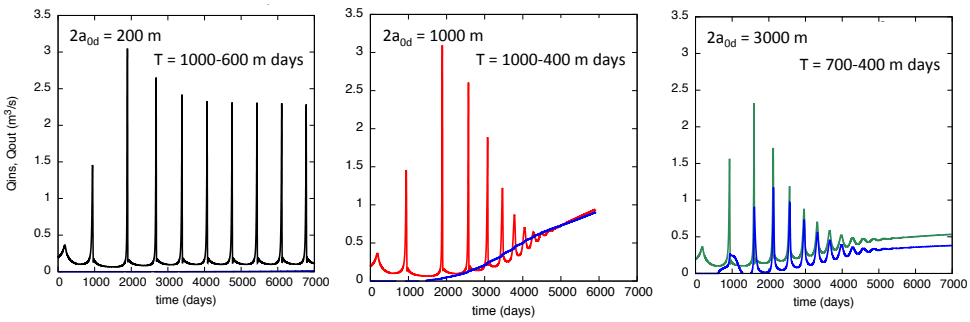

Shallow Chamber Volume

V_{chs} = 50 km^3

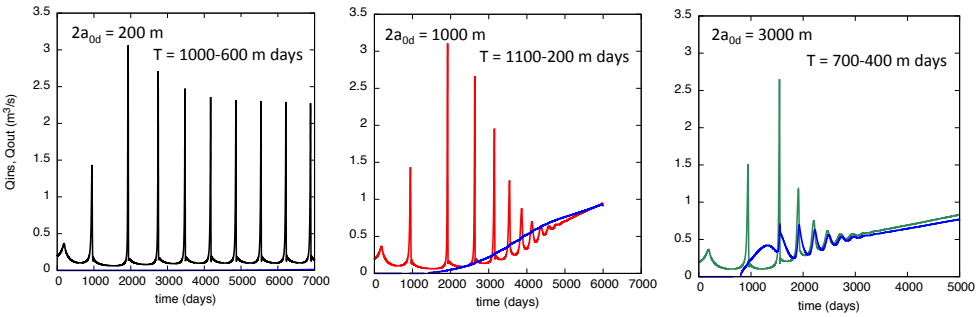

137

2

Fixed parameters
ARs = 1
ARd = 1
V_{chs} = 40 km^3

Deeper Chamber Volume

V_{chd} = 550 km^3

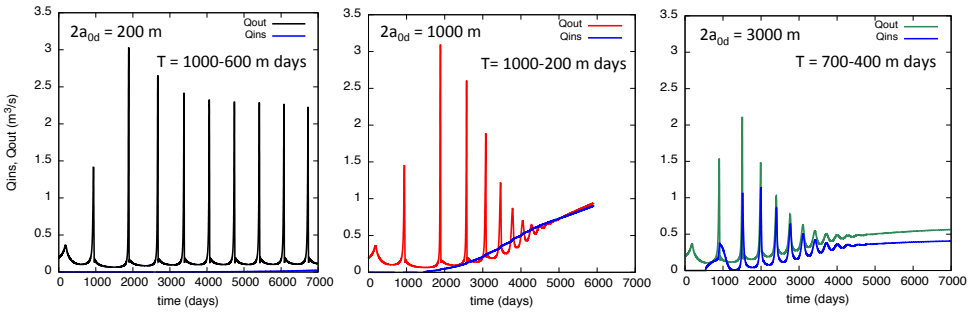

Deeper Chamber Volume

V_{chd} = 650 km^3

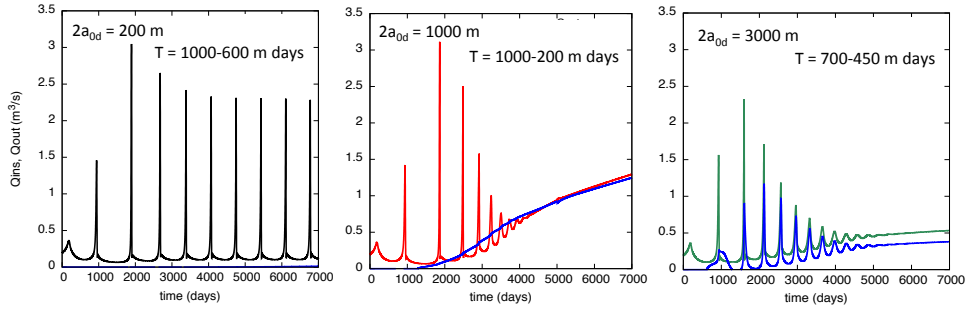

Deeper Chamber Volume

V_{chd} = 750 km^3

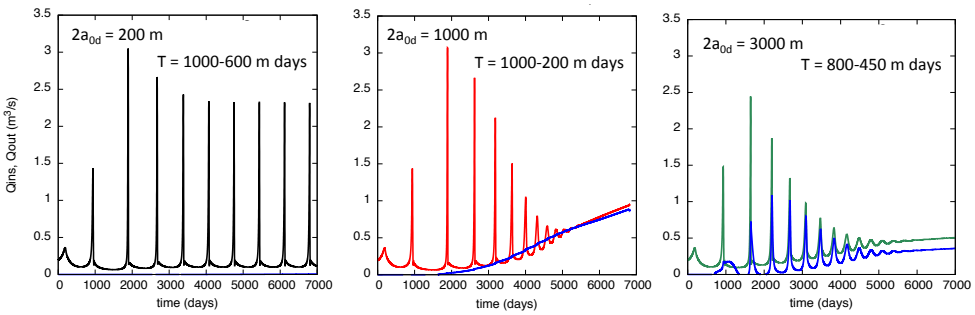

138

Fixed parameters : ARs = 1 ; ARd = 1; Vchd = 650 km³ ; Vchs = 40 km³

- *Qin_depth = 1 m³/s*

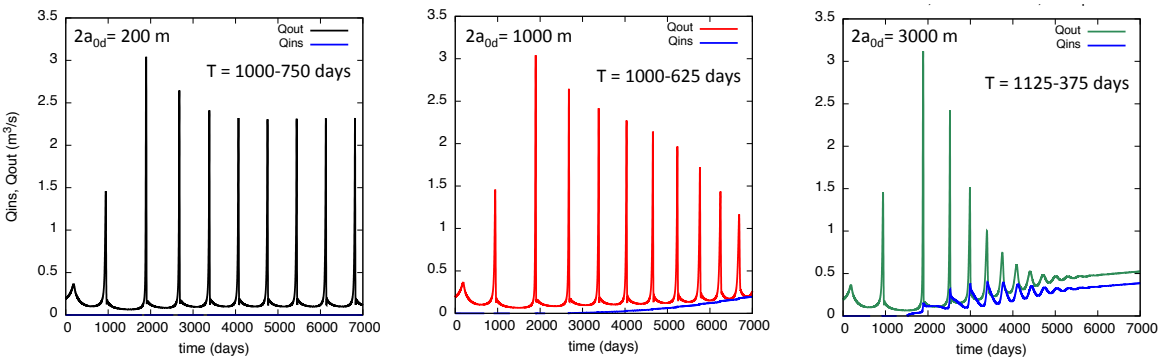

- *Qin_depth = 3 m³/s*

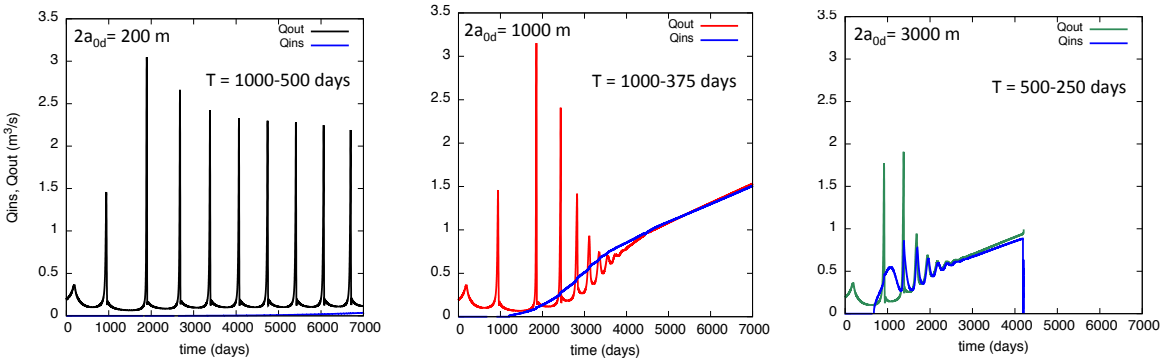

Appendix A4

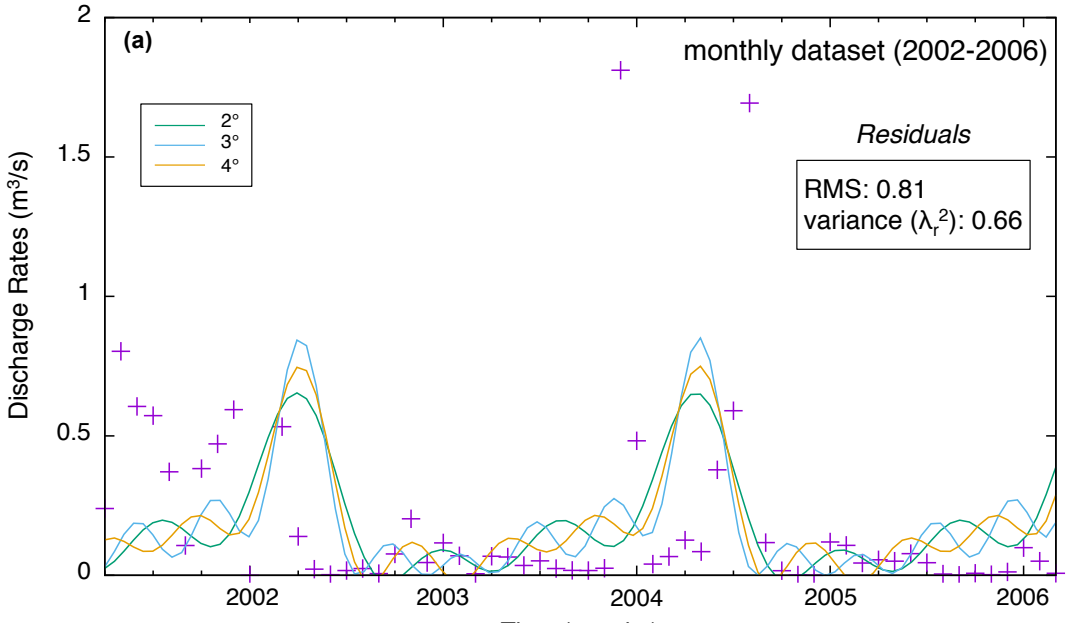
(a)
monthly dataset (2002-2006)
2°
3°
4°
Residuals
RMS: 0.81
variance (λ_r^2): 0.66
Discharge Rates (m^3/s)
2
1.5
1
0.5
0
2002
2003
2004
2005
2006

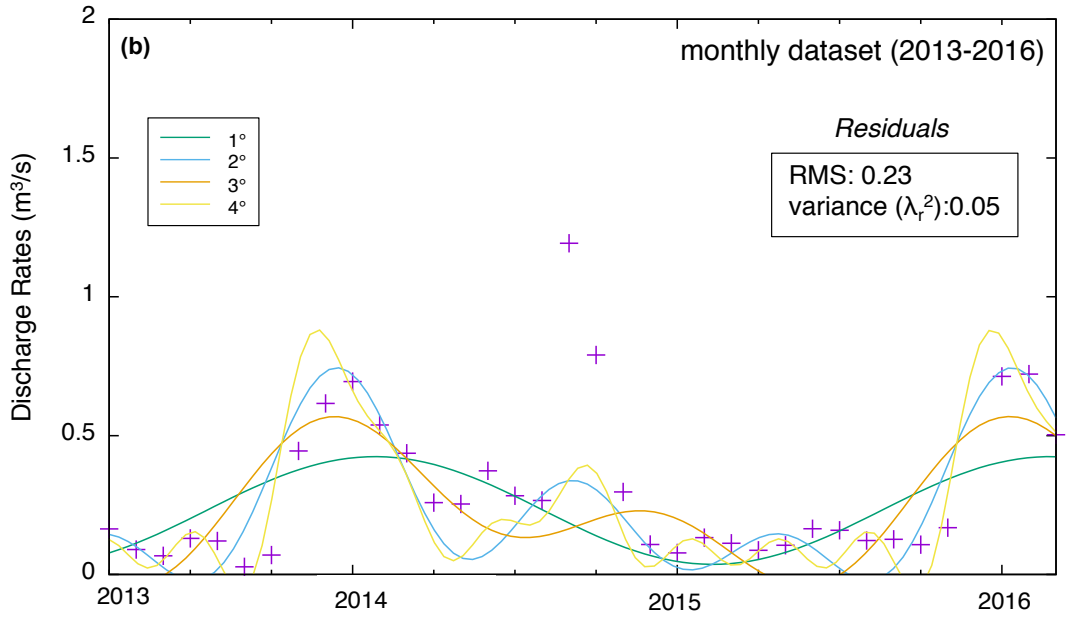
(b)
monthly dataset (2013-2016)
1°
2°
3°
4°
Residuals
RMS: 0.23
variance (λ_r^2):0.05
Discharge Rates (m^3/s)
2
1.5
1
0.5
0
2013
2014
2015
2016